



1 **Title:** Perturbation increases source-dependent organic matter degradation rates in estuarine  
2 sediments.

3

4 **Author information**

5 Guangnan Wu<sup>1</sup>, Klaas G.J. Nierop<sup>2</sup>, Bingjie Yang<sup>3</sup>, Stefan Schouten<sup>3</sup>, Gert-Jan Reichart<sup>1,2</sup>, Peter  
6 Kraal<sup>1</sup>

7

8 <sup>1</sup> Royal Netherlands Institute for Sea Research, Department of Ocean Systems, Landsdiep 4, 1797  
9 SZ 't Horntje, The Netherlands

10 <sup>2</sup> Utrecht University, Faculty of Geosciences, Princetonlaan 8a, 3584 CB Utrecht, The Netherlands

11 <sup>3</sup> Royal Netherlands Institute for Sea Research, Department of Marine Microbiology &  
12 Biogeochemistry, Landsdiep 4, 1797 SZ 't Horntje, The Netherlands

13

14 **Corresponding author**

15 Guangnan Wu ([guangnan.wu@nioz.nl](mailto:guangnan.wu@nioz.nl))

16

17

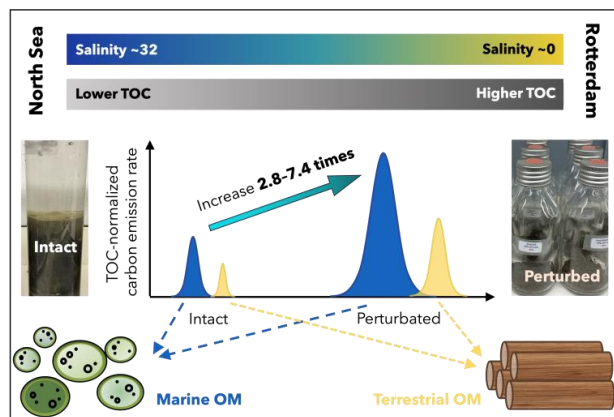


18 **Abstract**

19 Despite a relatively small surface area on Earth, estuaries play a disproportionately important role in  
20 the global carbon cycle due to their relatively high primary production and rapid organic carbon  
21 processing. Estuarine sediments are highly efficient in preserving organic carbon and thus often rich  
22 in organic matter (OM), highlighting them as important reservoirs of global blue carbon. Currently,  
23 these habitats are facing intensified human disturbance, one of which is sediment dredging. To  
24 understand estuarine carbon dynamics and the impact of perturbations, insights into sediment OM  
25 sources, composition, and degradability is required. We characterized the sediment OM properties  
26 and oxidation rates in one of the world's largest ports, the Port of Rotterdam, located in a major  
27 European estuary. Using a combination of OM source proxies and end-member modeling analysis,  
28 we quantified the contributions of marine (10–65%), riverine (10–60%), and terrestrial (10–65%) OM  
29 inputs across the investigated transect, with salinity ranging from 32 (marine) to almost 0 (riverine).  
30 Incubating intact sediment cores from two contrasting sites (marine versus riverine) suggested that  
31 OM was more reactive in marine sediment than riverine sediment. Exposing wet bulk surface  
32 sediment to atmospheric oxygen in a bottle incubation experiment showed a 2.8–7.4 times increase of  
33 OM degradation rates, while the impact of OM source and composition maintained the observed  
34 differences in rates between sites. This shows that sediment perturbation and the reintroduction of  
35 oxygen can substantially boost OM degradation. By combining detailed quantitative characterization  
36 of estuarine OM properties with degradation rates under different environmental conditions, our  
37 results further our understanding of the factors that govern OM degradation rates in (perturbed)  
38 estuarine systems. Ultimately, this contributes to constraining the impact of human perturbation on  
39 OM cycling in estuaries and its role in the carbon cycle.

40

41 **Graphical abstract**



42

43

44

45



46 **1. Introduction**

47 Estuaries are highly dynamic aquatic systems that are influenced by simultaneous marine, riverine,  
48 and terrestrial inputs. In this transition zone, strong and variable gradients exist in hydrodynamic and  
49 sediment properties, resulting in dynamic and complex cycles of key elements such as carbon  
50 through coupled physical, chemical, and biological processes (Barbier et al., 2011; Dürr et al., 2011;  
51 Laruelle et al., 2010). Despite representing only 0.03% of the surface area of marine systems,  
52 estuaries are estimated to release approximately 0.25 Pg carbon annually into atmosphere on a  
53 global scale, which is equivalent to 17% of the air-water CO<sub>2</sub> gas exchange of the entire open ocean  
54 (Bauer et al., 2013; Li et al., 2023). Additionally, estuarine sediments store large amounts of organic  
55 carbon (Macreadie et al., 2019; McLeod et al., 2011); due to high productivity and high sedimentation  
56 rates, carbon burial rates in estuaries are up to one order of magnitude higher than forest soils and  
57 three orders of magnitude higher than in open ocean sediments (Kuwae et al., 2016). Their  
58 disproportionally large importance in the global carbon cycle highlights the need to improve our  
59 understanding of carbon dynamics in estuarine systems.

60

61 Organic matter (OM), a fundamental component of sediment, plays a key role in sediment carbon  
62 fluxes and sequestration. The degradation of OM contributes to the release of carbon dioxide (CO<sub>2</sub>)  
63 and methane (CH<sub>4</sub>). It is a dynamic process that proceeds through a series of enzymatic reactions  
64 involving different organisms, oxidants, and intermediate compounds. Studies have pointed out the  
65 importance of OM characteristics in influencing the rate and extent of OM degradation (Burd et al.,  
66 2016; Burdige, 2007; LaRowe and Van Cappellen, 2011). For instance, extensively degraded OM and  
67 biopolymers such as cellulose and lignin are less susceptible to degradation than freshly produced  
68 nitrogenous compounds (Arndt et al., 2013). Estuarine systems have diverse terrestrial and aquatic  
69 OM sources, which exhibit varying degrees of degradability (Canuel and Hardison, 2016). Moreover,  
70 the interactions between OM and other components (organic or inorganic) during transportation,  
71 deposition, and mineralization can alter OM characteristics. Processes such as condensation,  
72 (geo)polymerization and mineral association increase the resistance to OM degradation, thereby  
73 promoting OM preservation (Wakeham and Canuel, 2006).

74

75 Sediment OM degradation is also influenced by ambient environmental conditions (Arndt et al., 2013;  
76 Burd et al., 2016; Burdige, 2007; LaRowe and Van Cappellen, 2011). The degradation pathway  
77 follows the sequential utilization of the terminal electron acceptors (TEAs), typically in the order of O<sub>2</sub>,  
78 NO<sub>3</sub><sup>-</sup>/NO<sub>2</sub><sup>-</sup>, Mn (IV), Fe (III) and SO<sub>4</sub><sup>2-</sup>, with a progressive decrease in energy yield down the redox  
79 ladder. The availability of these TEAs is greatly influenced by the depositional conditions. Estuaries  
80 are highly dynamic systems where strong and shifting salinity (i.e. sulfate) gradients exist. This can  
81 lead to a strong spatial variability in OM degradation pathways and carbon dynamics, particularly for  
82 CH<sub>4</sub> (Cao et al., 2021). Moreover, compilation of field data reveals that organic carbon burial efficiency  
83 varies substantially in space because the availability and exposure time of TEAs are influenced by  
84 environmental factors such as sedimentation rate (Arndt et al., 2013; Freitas et al., 2021). Estuaries  
85 are often characterized by relatively high sedimentation rates, with supply of riverine material that



86 settles under low flow velocities in deltas and estuaries as well as large inputs of (re)suspended  
87 marine matter from the coastal zone (ref). Oxygen transport into sediment is sufficiently low relative to  
88 the flux of reactive organic carbon to sediments to maintain very shallow oxygen penetrations depths,  
89 on the scale of micro- to millimeters (Burdige, 2012). By notably reintroducing O<sub>2</sub> to previously buried  
90 OM in oxygen-deficient environment, both naturally and anthropogenically induced sediment  
91 disturbance can change sediment redox chemistry and thereby have a profound effect on OM  
92 degradation pathways and burial efficiency (Aller, 1994).

93

94 Although estuaries have been widely studied from an ecological perspective, large variation in OM  
95 properties and cycling processes within and across estuarine systems contributes to the uncertainty in  
96 quantifying their significance in the global carbon cycle. This uncertainty is partially due to the highly  
97 diverse OM sources and properties in estuarine systems. Many studies of estuarine OM sources use  
98 bulk proxies such as the weight ratio of total organic carbon to total nitrogen (C/N ratio) and their  
99 stable isotope ratios ( $\delta^{13}\text{C}_{\text{org}}$  and  $\delta^{15}\text{N}$ ; (Canuel and Hardison, 2016; Carneiro et al., 2021; Cloern et  
100 al., 2002; Middelburg and Nieuwenhuize, 1998). In other studies, OM sources have been investigated  
101 by identifying biomarker compounds that are associated with specific sources and transformation  
102 processes. For example, the branched and isoprenoid tetraether (BIT) index, based on the relative  
103 abundance of terrestrially and/or freshwater derived branched glycerol dialkyl glycerol tetraether  
104 (GDGT) versus marine derived isoprenoid GDGT crenarchaeol, was adopted to quantify the relative  
105 contribution of terrestrial OM in sediments (Herfort et al., 2006; Hopmans et al., 2004; Smith et al.,  
106 2010; Strong et al., 2012). Some studies focused on macromolecular organic matter (MOM)  
107 composition in sediments to identify OM sources (Kaal et al., 2020; Nierop et al., 2017). Lignin, an  
108 important constituent of vascular plant MOM, has proved to be a useful tracer of vascular plant inputs  
109 to estuarine/coastal margin sediment (Bianchi and Bauer, 2012; Buurman et al., 2006; Fabbri et al.,  
110 2005; Hedges and Oades, 1997; Kaal, 2019). Furthermore, the relationship between OM source and  
111 degradability can be intricate, which inhibits our quantitative understanding of estuarine OM  
112 degradation.

113

114 Understanding the processing of OM within estuaries takes on further importance because many  
115 estuarine systems are intensively altered by human activities (Arndt et al., 2013; Heckbert et al.,  
116 2012; Holligan and Reiners, 1992). Dredging is a common sediment management practice in many  
117 coastal regions and rivers worldwide. More than 600 million m<sup>3</sup> of dredged material is generated  
118 annually just in Western Europe, China, and the USA (Amar et al., 2021). These anthropogenic  
119 perturbations expose buried sediment to an oxygenated environment, which is energetically favorable  
120 for OM degradation (LaRowe et al., 2020). The active sediment reworking on the Amazon shelf was  
121 reported to stimulate mineralization and decreased the sediment organic carbon content (Aller et al.,  
122 1996). Considering the massive amount of material being dredged, recent studies have suggested to  
123 explore the possibilities of reusing dredging sediment as construction materials (Brils et al., 2014).  
124 However, one of the great unknowns lies in the fate of the large amount of organic carbon stored in  
125 these sediments during dredging, drying, processing, and further use. Given that dredging activities



126 continue to increase driven by the increasing societal and economic needs (van de Velde et al.,  
127 2018), it is of great importance to understand to what extent anthropogenic sediment perturbations  
128 affect OM processing in and carbon emissions from estuarine sediments.

129

130 In this study, we investigate the spatial variability in OM content and properties and relationships  
131 between OM source, composition, and degradability along a salinity gradient in the profoundly  
132 disturbed Port of Rotterdam estuarine environment of the Rhine-Meuse delta system. Given the  
133 frequent dredging activities in our study area, which hosts a globally major port, we aim to understand  
134 the impact of sediment dredging and its potential land applications on carbon dynamics. We used a  
135 combination of bulk OM proxies, BIT index, macromolecular organic matter (MOM) composition  
136 analysis, as well as end-member modelling to understand OM sources and composition. Furthermore,  
137 organic matter degradation rates were estimated both in undisturbed sediment cores and in bottles  
138 incubation with wet sediment under atmospheric conditions, the latter as representative for dredged  
139 sediment. Our show that variability in OM sources and subsequently molecular properties, as well as  
140 perturbation (i.e. introduction of oxygen), have important effects on OM degradation rates. We show  
141 that in addition to content, the properties of OM influences carbon emissions from estuarine sediment  
142 and the carbon footprint of anthropogenic perturbations.

143

## 144 **2. Materials and methods**

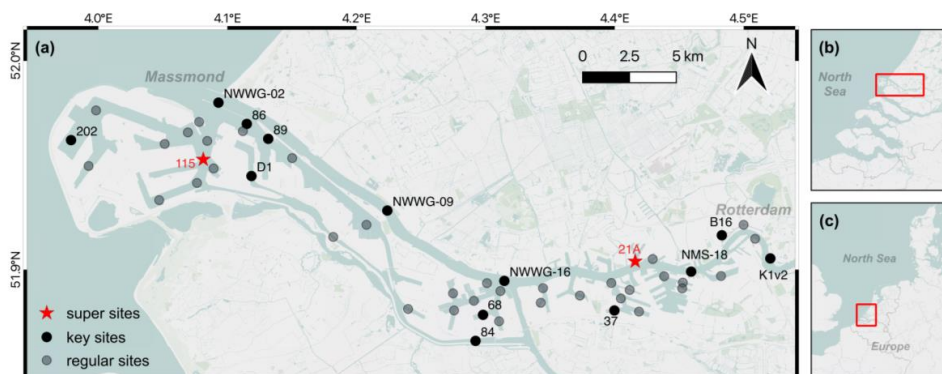
### 145 **2.1. Study area and sample collection**

146 Our study area is located in the northern part of the Rhine-Meuse estuary (Fig. 1), spanning from  
147 Rotterdam city to the Maasmond. This area representing a transitional environment from riverine to  
148 marine is heavily urbanized and hosts one of the world's largest ports, the Port of Rotterdam (PoR).  
149 Every year, large amounts of sediment are deposited in the harbor from both rivers as well as the  
150 North Sea (Kirichek and Rutgers, 2020). The water channel maintenance and harbor expansion lead  
151 to an increasing need of sediment dredging. Currently, over 10 million m<sup>3</sup> of dredged materials are  
152 relocated to the shallow North Sea, while around 1.5 million m<sup>3</sup> are being stored as contaminated  
153 sediment in a holding basin in the PoR area (Kirichek and Rutgers, 2020).

154

155 We collected bulk sediments from 49 locations throughout the study area (Fig. 1) in the summer of  
156 2021. Sediments down to ~50 cm depth were collected using a gravity corer (ø9 cm). Once on deck,  
157 materials in the corer were emptied into 5-L polypropylene buckets that were closed and stored in the  
158 fridge at 4 °C. These samples, later referred as bulk sediments, were further processed within a week  
159 after collection at the Royal Netherlands Institute for Sea Research (NIOZ) on Texel, the Netherlands.  
160 In addition to bulk sediments, intact sediment cores were collected in summer 2022 upon revisiting  
161 two contrasting sites (referred as 'super sites' in Fig. 1) in the marine (site 115, salinity 28.7) and  
162 riverine (site 21A, salinity 5.1) realm of the PoR area. The intact sediment cores were immediately  
163 cooled, transported back to the NIOZ and used in whole-core incubation experiments (see section  
164 2.5) within 5 hours after collection.

165



166  
167 **Fig. 1.** (a) The investigated study area and sampling sites. Sediments from all 49 sites were subjected  
168 to bulk analysis as detailed in section 2.2. Sediments from 13 key sites were used for lipid and MOM  
169 analysis as detailed in section 2.3 and 2.4, respectively. Sediment cores from two super sites were  
170 used in a whole-core incubation experiment as detailed in section 2.5. (b) The location of investigated  
171 study area in the Rhine–Meuse estuary. (c) The location of Rhine–Meuse estuary in Western Europe.  
172 Map created using QGIS software. Basemap courtesy of Mapbox.

173

## 174 2.2. Sample processing and analysis

175 Bulk sediments were thoroughly mixed using a spatula in the buckets. Approximately 40 mL of wet  
176 sediment were transferred into 50-mL polypropylene centrifuge tubes (Falcon) and centrifuged at  
177 3000 rpm for 20 min (Hermle Z 446). In a N<sub>2</sub>-purged glove bag, the porewater was immediately  
178 filtered through a 0.45- $\mu$ m nylon syringe filter (MDI). Salinity was estimated by comparing the  
179 porewater sodium (Na) concentration to the average seawater sodium concentration and salinity in  
180 the North Sea (Ijsseldijk et al., 2015; Steele et al., 2010). For Na analysis, the porewater was diluted  
181 around 900 times in 1 M double-distilled HNO<sub>3</sub> and analyzed by inductively coupled plasma mass  
182 spectrometry (ICP-MS, Thermo Scientific, Element 2).

183

184 The centrifuge tubes with wet sediment residues after centrifugation were purged with N<sub>2</sub> and stored  
185 at -20 °C in N<sub>2</sub>-purged, gas-tight Al-laminate bags to prevent oxidation. To prepare for subsampling,  
186 the sediment residues were thawed overnight in a N<sub>2</sub>-purged glove bag (Coy Laboratories) and  
187 subsequently homogenized. One portion of wet sediment residue (~1 g) was mixed with 50 mL of 3 g  
188 L<sup>-1</sup> sodium pyrophosphate solution and gently shaken to disaggregate particles. Particle size  
189 distribution was determined using a Coulter laser particle sizer (Beckman Coulter), from which  
190 percentages of clay (0–2  $\mu$ m), silt (2–63  $\mu$ m), sand (63–2000  $\mu$ m) and the median particle size (D50)  
191 were calculated.

192

193 Approximately 10 g wet sediment residue was freeze-dried (Hetosicc freeze dryer) for 72 h and  
194 manually ground with an agate pestle and mortar, and further subsampled for carbon and nitrogen  
195 (CN) analysis. One subsample of the freeze-dried sediment (~10 mg) was directly used for measuring



196 total nitrogen (TN) and stable nitrogen isotope composition (expressed as  $\delta^{15}\text{N}$ , relative to  
197 atmospheric nitrogen) by a CN elementary analyzer (Thermo Scientific, FLASH 2000) coupled to a  
198 Delta V Advantage isotope ratio mass spectrometer (Thermo Scientific). Another freeze-dried  
199 subsample (~0.5 g), firstly treated with 1 M HCl to remove carbonates, was used for measuring total  
200 organic carbon (TOC) and stable carbon isotope composition (expressed as  $\delta^{13}\text{C}_{\text{org}}$ , relative to Vienna  
201 Pee Dee Belemnite). Certified laboratory standards (acetanilide, urea, and casein) were used for  
202 calibration with each sample. Precision and accuracy for standards and triplicate samples were  
203  $\pm 0.3\text{‰}$  for  $\delta^{13}\text{C}_{\text{org}}$  and  $\delta^{15}\text{N}$ , and the relative standard deviation (RSD; standard deviation/mean) was  
204  $< 10\%$  for TOC and TN.

205

### 206 **2.3. Lipid extraction and analysis**

207 Freeze-dried and homogenized sediments (2–10 g) from 13 key locations (Fig. 1) were ultrasonically  
208 extracted with dichloromethane (DCM):methanol (2:1, v:v) five times. For each sample, extracts  
209 obtained from the five steps were combined. The total extract was separated over an  $\text{Al}_2\text{O}_3$  column  
210 into an apolar, neutral and polar fraction using hexane:DCM (9:1, v:v), hexane:DCM (1:1, v:v) and  
211 DCM:methanol (1:1, v:v), respectively. The polar fractions containing glycerol dialkyl glycerol  
212 tetraethers (GDGTs) were dried under  $\text{N}_2$ , dissolved in hexane:propanol (99:1, v:v), and filtered using  
213 a 0.45  $\mu\text{m}$  PTFE filter. This fraction was subsequently analyzed with an ultra-high performance liquid  
214 chromatography mass spectrometry (UHPLC-MS) on an Agilent 1260 Infinity HPLC coupled to an  
215 Agilent 613MSD according to (Hopmans et al., 2016). The isoprenoid and branched GDGTs were  
216 detected by scanning for their  $[\text{M}+\text{H}]^+$  ions. The BIT index was calculated according to (Hopmans et  
217 al., 2004).

218

### 219 **2.4. Macromolecular organic matter (MOM) isolation and analysis**

220 The sediment residues after lipids extraction were dried under  $\text{N}_2$ . To isolate MOM, dried sediment  
221 residue (2–3 g) was transferred into 50-mL centrifuge tubes and decalcified with 30 mL 1 M HCl for 4  
222 h, later rinsed twice with 25 mL milli-Q water (18 M $\Omega$ ). After centrifugation and decanting the  
223 supernatant, 15 mL 40% HF (analytical grade, Merck) was added and shaken for 2 h at 100 rpm. The  
224 solution was diluted with milli-Q water to 50 mL and left standing overnight, after which the solution  
225 was decanted. A volume of 15 mL 30% HCl was added and subsequently diluted with milli-Q water to  
226 50 mL. After shaking for 1 h and centrifugation, the solution was decanted, and the residues were  
227 washed with milli-Q water three times to neutralize pH and subsequently freeze-dried. Samples were  
228 desulfurized using activated copper pellets in DCM. Suspensions were stirred overnight after which  
229 the copper pellets and DCM were removed, and the MOM was air-dried prior to the analysis.

230

231 The analysis of MOM was conducted at Utrecht University using the pyrolysis-gas chromatograph-  
232 mass spectrometry method previously described in (Nierop et al., 2017). In short, the isolated MOM  
233 was pyrolyzed on a Horizon Instruments Curie-Point pyrolysis unit. The pyrolysis unit was connected  
234 to a Carlo Erba GC8060 gas chromatograph and the products were separated by a fused silica  
235 column (CP-Sil5, 25 m, 0.32 mm i.d.) coated with CP-Sil5 (film thickness 0.40  $\mu\text{m}$ ). The column was



236 coupled to a Fisons MD800 mass spectrometer. Pyrolysis products were identified using a NIST  
237 library or by interpretation of the spectra, by their retention times and/or by comparison with literature  
238 data. Quantification was performed according to (Nierop et al., 2017).

239

## 240 **2.5. Whole-core sediment incubation**

241 Triplicate intact sediment cores collected from sites 115 and 21A were used for whole-core incubation.  
242 Prior to incubation, cores were carefully manipulated to have ~15 cm of undisturbed top sediment with  
243 ~20 cm of overlying water. After confirming that the sediment surface was not disturbed, an oxygen  
244 sensor spot (Presens) was attached to the inner wall of the core tube (5 cm from the top) to monitor  
245 O<sub>2</sub> in the overlying water. The cores, capped at the bottom and open at the top, were submerged in  
246 bottom water from the corresponding site in an incubation tank. Stirrers were placed in each core to  
247 mix the overlying water (at ~1 rpm) and the cores were left open overnight to equilibrate. The water in  
248 the tank was kept fully oxygenated by sparging with air using an aquarium pump. Temperature in the  
249 room was maintained at the measured site bottom water temperature (19 °C). At the start of the  
250 incubation, the cores were capped with gas-tight lids with an outlet to sample bottom water in core  
251 and an inlet to replace sampled volume with site water from a 20-L reservoir. Over the course of an  
252 eight-hour incubation period, 30 mL of bottom water were extracted at pre-determined time intervals  
253 of 0, 1.5, 3.5, 5, 6.5, and 8 h. The dissolved O<sub>2</sub> concentration in the overlying water in each core was  
254 measured every five minutes using the sensor spots and a Presens OXY-4 SMA meter with fiber optic  
255 cables, operated using Presens Measurement Studio 2. Immediately after sampling, the water  
256 samples were filtered using 0.45-µm nylon syringe filters for dissolved inorganic carbon (DIC) and  
257 dissolved inorganic nitrogen (DIN: NH<sub>4</sub><sup>+</sup>, NO<sub>3</sub><sup>-</sup>, NO<sub>2</sub><sup>-</sup>) analysis, while an unfiltered subsample was  
258 retained for methane (CH<sub>4</sub>) analysis.

259

260 The DIC samples were diluted 10 times in N<sub>2</sub>-purged 25 g L<sup>-1</sup> sodium chloride solution without  
261 headspace and analyzed within 24 hours by a continuous flow analyzer (QuAAtro, Seal Analytical).  
262 The DIN samples were stored at -20 °C and later analyzed by a continuous flow analyzer (TRAACS  
263 800+). For CH<sub>4</sub>, 12 mL of bottom water was directly transferred into a 12 mL Exetainer vial (Labco),  
264 immediately poisoned with ~0.25 mL of saturated zinc chloride solution and capped with a butyl  
265 rubber stopper ensuring no headspace was present. Dissolved CH<sub>4</sub> concentration was determined  
266 using a headspace technique (Magen et al., 2014). Prior to the measurement, 1 mL of N<sub>2</sub> headspace  
267 was injected through the stopper in each Exetainer vial while a needle allowed the equivalent volume  
268 of sample to escape, after which the samples were equilibrated for a week. Headspace CH<sub>4</sub>  
269 concentrations were then measured by a gas chromatograph (Thermo Scientific FOCUS GC)  
270 equipped with a HayeSep Q Packed GC Column and a flame ionization detector. A calibrated curve  
271 was made using a certified 1000 ppm CH<sub>4</sub> standard (Scott Specialty Gases Netherlands B.V.). From  
272 the measured CH<sub>4</sub> concentration in the headspace, the total dissolved CH<sub>4</sub> in the bottom water was  
273 calculated using the equations in (Magen et al., 2014) with the Bunsen coefficient (Yamamoto et al.,  
274 1976). Benthic fluxes of DIC and CH<sub>4</sub> were calculated using the concentration changes of solutes in





275 the bottom water of closed cores during the incubation period, as determined by linear regression  
276 analysis of the individual time series.

277

## 278 **2.6. Subaerial incubation of dredged sediment**

279 The subaerial incubation experiments were conducted in triplicate for six sediments (115, 21A, 86,  
280 B16, NWWG-02 and K1v2). Freeze-dried and homogenized sediment (~10 g) was transferred into a  
281 330-mL borosilicate glass bottle, leading to a thin layer (less than 5 mm) of sediment. The moisture  
282 level of sediment was adjusted with artificial rainwater (composition detailed in Table S1 in  
283 Supplementary Information (SI)) to ensure a water-filled pore space at 60% according to (Fairbairn et  
284 al., 2023). The sediment was incubated in the dark at room temperature (20 °C). The CO<sub>2</sub> emission  
285 rate was measured on day 2, 6, 9, 16, 23, 30 and 37. On the day of measurement, bottles were  
286 sealed with rubber stoppers tightened with aluminum crimp caps for approximately 3 hours. We  
287 measured the CO<sub>2</sub> concentrations in the headspace immediately after the bottles were capped and  
288 approximately 3 hours later. The CO<sub>2</sub> accumulation in the headspace of each bottle during these 3  
289 hours was used to calculate a CO<sub>2</sub> emission rate. For the rest of the time, bottles were kept open to  
290 the atmosphere. The moisture level was maintained once a week and varied by less than 10% from  
291 the target value.

292

293 The CO<sub>2</sub> measurement for the subaerial incubation was conducted by withdrawing a volume of 150  
294 µL headspace gas using a 250-µL glass, gas-tight syringe (Hamilton). The headspace sample was  
295 immediately injected into a gas chromatograph (GC, Agilent, 8890 GC system) equipped with a  
296 Jetanizer and a flame ionization detector. Gases were carried by helium and separated by a  
297 Carboxen-1010 PLOT analytical column (Sigma-Aldrich). Calibration was conducted by using certified  
298 reference CO<sub>2</sub> gas (Scott specialty gases, Air Liquide, Eindhoven, The Netherlands).

299

300 To determine the percentage of degraded TOC over time, we firstly calculated the cumulative amount  
301 of CO<sub>2</sub> emission and then normalized it to the total amount of organic carbon in the incubated  
302 sediments, calculated from the dry sediment mass and its TOC content. The cumulative CO<sub>2</sub> emission  
303 was obtained by integrating the CO<sub>2</sub> emission rate over time. For days when CO<sub>2</sub> emission rates were  
304 not measured, the rates were estimated using spline interpolation. The integration and normalization  
305 were performed using the 'AUC' (area under curve) function in RStudio.

306

## 307 **2.7. End-member modelling of OM sources**

308 The contribution of three major OM end-members (marine, riverine, and terrestrial OM) to the  
309 sediment was quantified based on  $\delta^{13}\text{C}_{\text{org}}$  and C/N ratio using a Bayesian mixing model, MixSIAR  
310 (Stock et al., 2018). Anthropogenic OM such as petroleum and coal products were not considered as  
311 they typically have a much higher C/N ratio (Tumuluru et al., 2012) compared to our samples (mostly  
312 <20), thus suggesting a limited contribution. Input from industrial and chemical waste is considered  
313 being minimal because >90% of sediment is regarded as clean/safe with organic contaminants below  
314 their national intervention values (Kirichek and Rutgers, 2020). We did not include sewage OM and



315 agricultural wastes as separate end-members due to their high variability in  $\delta^{13}\text{C}_{\text{org}}$  ( $-28\text{‰}$ – $-23\text{‰}$ ;  
 316 (Shao et al., 2019)) and C/N ratio (Chow et al., 2020; Puyuelo et al., 2011; Szulc et al., 2021), and the  
 317 values are largely overlaps with those of the considered three end-members. The model incorporates  
 318 the common ranges of three OM end-members in coastal environment (Table 1) and employs Markov  
 319 Chain Monte Carlo (MCMC) simulation to sample from the posterior distribution. The distribution  
 320 provides estimates of the mean contribution with standard deviation. The model was run in RStudio  
 321 with package “MixSIAR” integrated into the JAGS program.

322

323 **Table 1.** Mean values and standard deviations of  $\delta^{13}\text{C}_{\text{org}}$  and C/N ratio of three OM end-members  
 324 used in the MixSIAR analysis. Values from literature (Bianchi and Bauer, 2012; Finlay and Kendall,  
 325 2007; Lamb et al., 2006).

End-member	Typical OM	$\delta^{13}\text{C}_{\text{org}}$ (‰)	C/N
Marine OM end-member	Marine POC, algae, bacteria	$-20\pm 4$	$7\pm 3$
Riverine OM end-member	Freshwater POC, algae, bacteria	$-29\pm 4$	$7\pm 3$
Terrestrial OM end-member	Vegetation, soil OM, bacteria	$-26.5\pm 5.5$	$30\pm 18$

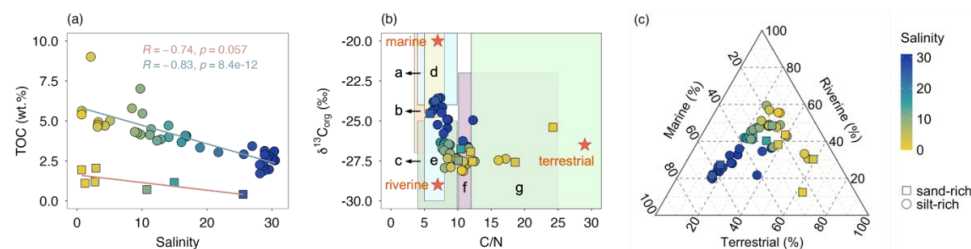
326

### 327 3. Results

#### 328 3.1 Bulk geochemical feature of sediments

329 The PoR sediments were mostly (42 out of 49 samples) silt-rich with D50 smaller than  $20\ \mu\text{m}$ . A  
 330 salinity gradient was observed in the study area increasing from approximately 0 at the most eastern  
 331 part (Rotterdam city) to approximately 32 at the river mouth in the west. We observed a decrease in  
 332 TOC content with increasing salinity (Fig. 2a). The silt-rich sediments generally contained more than  
 333 2.5 wt.% TOC, with significantly lower TOC contents in the sand-rich sediments ( $p < 0.01$ , Student's  $t$ -  
 334 test). The weight ratio of C/N was between 5 and 13 for most samples (45 out of 49), and the  
 335 corresponding  $\delta^{13}\text{C}_{\text{org}}$  was in the range of  $-29\text{‰}$  to  $-23\text{‰}$  (Fig. 2b). Despite a weak correlation  
 336 between C/N ratio and  $\delta^{13}\text{C}_{\text{org}}$  ( $R = -0.38$ , Pearson), both properties showed (moderately) strong  
 337 trends against salinity (C/N ratio:  $R = -0.66$ ;  $\delta^{13}\text{C}_{\text{org}}$ :  $R = 0.68$ , Pearson; Fig. 2b).

338



339

340 **Fig. 2.** Bulk geochemical properties of 49 sediment samples from the PoR. (a) TOC vs. salinity for  
 341 both silt-rich ( $D50 < 20\ \mu\text{m}$ ) and sand-rich ( $D50 > 50\ \mu\text{m}$ ) sediments. (b)  $\delta^{13}\text{C}_{\text{org}}$  and the weight ratio of  
 342 C/N in sediments along salinity gradient in contrast to the typical  $\delta^{13}\text{C}_{\text{org}}$  and C/N ranges for OM from  
 343 coastal sediments in literature (Bianchi and Bauer, 2012; Finlay and Kendall, 2007; Lamb et al.,  
 344 2006): **a** marine POC, **b** bacteria, **c** freshwater POC, **d** marine algae, **e** freshwater algae, **f** soil OM, **g**



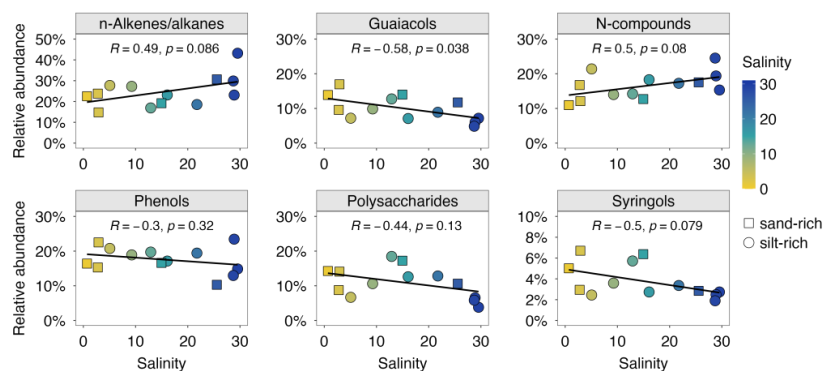
345 C<sub>3</sub> terrestrial plants. Asteroid signs represent the mean values of three OM sources used in end-  
346 member analysis. (c) The contribution (%) of marine, riverine and terrestrial OM using a mixing model.  
347 The standard deviation (10–25%) is provided in the Supplementary Information (SI, Table S1).

348

### 349 3.2. Flash pyrolysis products of MOM

350 Pyrolysis of isolated MOM produced hundreds of pyrolysis compounds. The identified pyrolysis  
351 products are listed in Supplementary Information (Table S2). They were divided into nine groups  
352 based on the chemical characteristics, following the approach detailed in Nierop et al. (2017). Here in  
353 Fig. 3, we present the relative abundance of six MOM pyrolysate groups along the salinity gradient,  
354 including *n*-alkenes/alkanes, guaiacols, N-compounds, phenols, polysaccharide-derived products, and  
355 syringols. The other three groups: phytadienes and pris-1-ene were only minor constituents (relative  
356 abundance < 5%), and aromatics showed a negligible correlation with salinity ( $-0.1 < R < 0.1$ ,  
357 Pearson; Fig. S1). With increasing salinity, we observed an increase in the relative abundance of *n*-  
358 alkenes/alkanes and N-compounds, while guaiacols, phenols, polysaccharides, and syringols  
359 decreased. The correlations were generally moderate or weak, as suggested by the magnitude of the  
360 correlation coefficient ( $-0.6 < R < 0.6$ , Pearson). Additionally, the correlation coefficients between the  
361 identified MOM pyrolysate groups and other bulk sediment properties (i.e. D<sub>50</sub>, C/N,  $\delta^{13}\text{C}_{\text{org}}$ ) were  
362 also weak (see SI, Fig. S2).

363



364

365 **Fig. 3.** The relative abundance of six groups of MOM pyrolysis products. Pearson correlation  
366 coefficient ( $R$ ) measures the strength of the linear relationship between grouped pyrolysates and  
367 salinity.

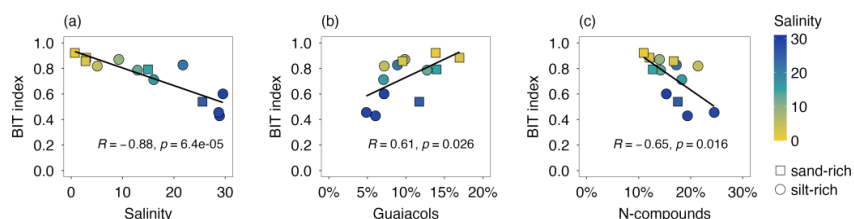
368

### 369 3.3. BIT index

370 Crenarchaeol and branched GDGTs were detected in sediments from all 13 investigated sites. The  
371 calculated BIT index ranged between 0.43 and 0.92 (Fig. 4a). A strong negative correlation was  
372 observed between BIT index and salinity ( $R = -0.88$ , Pearson) and between BIT index and  $\delta^{13}\text{C}_{\text{org}}$  ( $R$   
373 =  $-0.83$ , Pearson). In contrast, the correlation with MOM pyrolysis products were in general weak or  
374 moderate ( $-0.6 < R < 0.6$ , Pearson; Fig. S2), except for guaiacols and N-compounds (Fig. 4b & 4c).



375 Additionally, we did not observe significant difference between sand-rich and silt-rich sediments in BIT  
376 index values ( $p > 0.5$ , Student's *t*-test).  
377



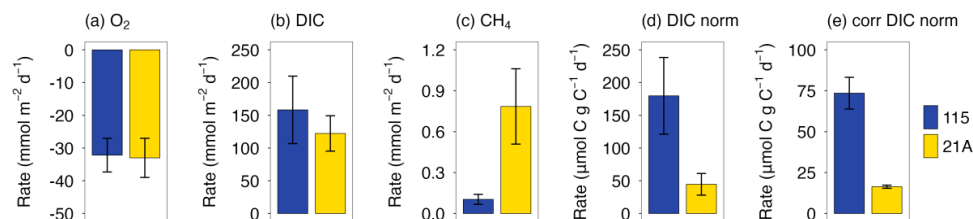
378  
379 **Fig. 4.** The BIT index of 13 sediments against (a) salinity, (b) relative abundance of guaiacols, (c)  
380 relative abundance of N-compounds.

381

#### 382 3.4. Benthic fluxes on intact sediment cores

383 During the whole-core incubation, the  $O_2$  concentration in the overlying decreased linearly from  
384 around 90% to 60% air-saturation for both the high salinity location (115, salinity 28.7, later referred as  
385 'marine' location) and the low salinity location (21A, salinity 5.1, later referred as 'riverine' location; SI  
386 Fig. S2). At the same time, concentrations of DIC and  $CH_4$  in the overlying water increased linearly  
387 with time (Fig. S2). Benthic  $O_2$  consumption rates were very similar at the two contrasting locations,  
388 around  $30 \text{ mmol m}^{-2} \text{ d}^{-1}$  (Fig. 5a). However, DIC was released into the overlying water at a much  
389 higher rate (i.e. 3–4 times larger than  $O_2$  consumption rate, Fig. 5b). The marine location (sediment  
390 115) showed a larger DIC efflux than the riverine location (sediment 115), but the difference was  
391 insignificant ( $p > 0.05$ , Student's *t*-test). Additionally, the  $CH_4$  efflux was one to two orders of  
392 magnitude smaller than the  $O_2$  and DIC fluxes and showed significant differences between two  
393 contrasting locations: the  $CH_4$  efflux at the river location was more than five times higher compared to  
394 the marine location (Fig. 5c).

395



396  
397 **Fig. 5.** Benthic fluxes of dissolved  $O_2$  (a), DIC (b), and  $CH_4$  (c) determined from whole-core incubation.

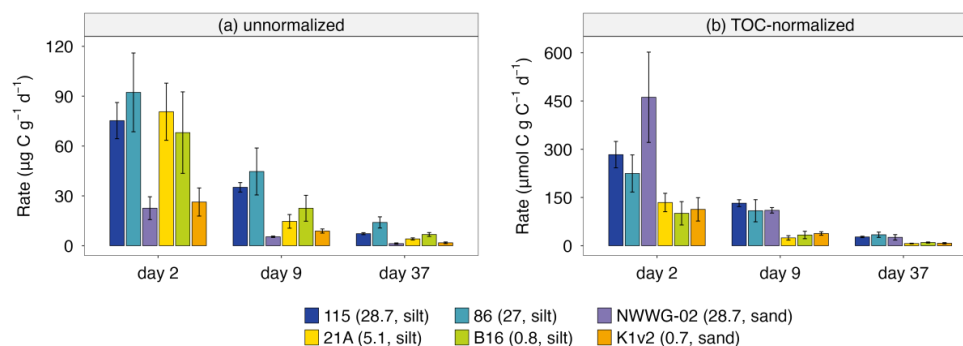
398 Positive and negative rates represent efflux (from sediment into overlying water) and influx (from overlying  
399 water into sediment), respectively. Sediment TOC-normalized DIC (DIC norm) is presented in panel (d)  
400 with TOC content being 2.2 wt.% for 115 and 5.0 wt.% for 21A. Panel (e) shows the OM-derived DIC,  
401 corrected with DIN (see SI) and normalized by sediment TOC (corr DIC norm).

402

#### 403 3.5. Carbon emissions on bulk sediments



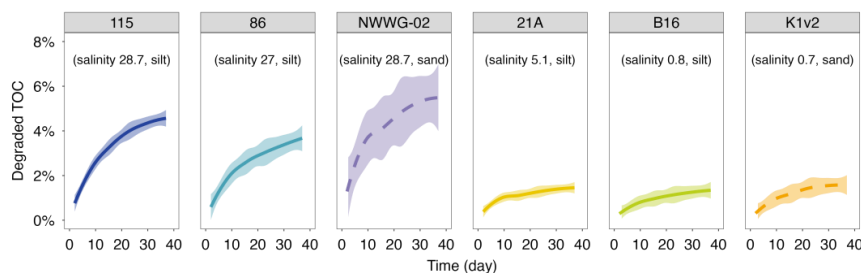
404 During the aerobic incubation experiment, CO<sub>2</sub> accumulation was detected during the 3-hour rate  
405 measurements for all timesteps. The CO<sub>2</sub> emission rate, expressed as  $\mu\text{g C g}^{-1} \text{ day}^{-1}$ , was the highest  
406 at the start of the incubation. The rates dropped drastically in the first two weeks and then stabilized  
407 after day 25. Here we present carbon emission rates at three timesteps representing the initial stage,  
408 declining stage, and stable stage (Fig. 6). The silt-rich sediments showed both higher emission rates  
409 throughout the incubation period (up to  $120 \mu\text{g C g}^{-1} \text{ day}^{-1}$ ) and stronger decreases in rate over time  
410 (more than  $60 \mu\text{g C g}^{-1} \text{ day}^{-1}$ ), compared to sand-rich sediments (maximum rate around  $35 \mu\text{g C g}^{-1}$   
411  $\text{day}^{-1}$ ; Fig. 6a). The TOC-normalized carbon emission rates were higher (up to three times) in the  
412 three marine sediments (salinity 27–28) compared to the three riverine sediments (salinity 0–5)  
413 throughout the experiment (Fig. 6b).



414 **Fig. 6.** Carbon emission rates in aerobic incubation at day 2, day 9 and day 37 from six sediments.  
415 Note the different scales and units for the y-axis for unnormalized rate (a) and TOC-normalized rate  
416 (b). Salinity and sediment texture are indicated in brackets in the legend.

417  
418  
419 The decreasing trend of CO<sub>2</sub> emission rate was also reflected in the cumulative percentage of  
420 degraded TOC over time (Fig. 7), which increased fast initially and stabilized towards the end of the  
421 incubation experiment. After the 37-day incubation period, the amount of degraded TOC ranged  
422 between 1 to 7% for the investigated sites. Additionally, the percentage of degraded TOC was 2–4  
423 times higher in sediments from marine locations than those in river locations, consistent with the  
424 differences in carbon emission rates (Fig. 6b).

425



426



427 **Fig. 7.** The percentage of degraded TOC over time in aerobic incubation experiments. The shading  
428 areas represent the 95% confidential interval for the fitted locally estimated scatterplot smoothing  
429 (LOESS) curves.

430

#### 431 **4. Discussion**

##### 432 **4.1 Organic matter content, source and composition in estuarine sediments**

433 The PoR sediments are characterized by relatively high TOC contents compared to North Sea surface  
434 sediments (0.03–2.79 wt.%; (Wiesner et al., 1990)), but in the range of Dutch coastal sediments (0–  
435 9.8 wt.%; (Stronkhorst and Van Hattum, 2003)) or other harbor systems such as the Port of Hamburg  
436 (2–7.6 wt.%; (Zander et al., 2020)). The high carbon contents arise from high productivity and rapid  
437 burial of OM under high sedimentation rates; oxygen penetration is limited into rapidly accumulating,  
438 organic-rich sediment and this most OM breakdown occurs via relatively slow, anaerobic processes  
439 (Schulz and Zabel, 2006). Moreover, the fine sediment texture observed at most investigated sites will  
440 limit oxygen diffusion and provides more sorption surface for OM (Keil et al., 1994), both contributing  
441 to the preservation of sediment OM and thus high TOC content compared to sandy sediment. This is  
442 expressed in the relatively low OM content of the coarser-grained sediments that were included in our  
443 study (Fig. 2a). Besides the clear impact of grain size on OM content, we observed a general  
444 decreasing trend in sediment TOC contents from river to marine area for PoR sediments, in line with  
445 previous work on estuarine sediment OM (Strong et al., 2012). The relatively low OM content in  
446 sediment from the marine-dominated sites in part arises from the large input (up to 5.7 million tons per  
447 year) in this area of repeatedly resuspended, OM-poor coastal sediment transported by strong tide  
448 and waves (Cox et al., 2021). Furthermore, moving downstream from the riverine to the marine part of  
449 estuarine systems, the contribution of OM-rich riverine sediment not only decreases but continuing  
450 OM degradation in this transported sediment further diminishes riverine supply of OM from the  
451 hinterland (Bianchi et al., 2018; Freitas et al., 2021). A confounding factor may be that OM burial and  
452 degradation are not only affected by inputs and sediment properties as described above, but also by  
453 the source and inherent properties of the OM.

454

455 The  $\delta^{13}\text{C}_{\text{org}}$  and C/N ratio have been widely used to assess OM sources in coastal environments  
456 (Canuel and Hardison, 2016; Lamb et al., 2006; Li et al., 2021; Middelburg and Nieuwenhuize, 1998).  
457 The OM in the estuarine ecosystems can originate from multiple sources, and the typical ranges of  
458  $\delta^{13}\text{C}_{\text{org}}$  and C/N ratio for the common OM sources are indicated in Fig. 2b. The trends in  $\delta^{13}\text{C}_{\text{org}}$  and  
459 C/N ratio suggest that OM in the PoR sediments is derived from a mixture of marine, riverine and  
460 terrestrial OM that are sourced from algae, bacteria, soil OM, and terrestrial plants, the relative  
461 contribution of these sources being a function of depositional conditions (riverine versus marine) as  
462 reflected by salinity (Fig. 2b). The observed  $\delta^{13}\text{C}_{\text{org}}$  values (–29––23‰) and their trend against salinity  
463 are similar to those in the broader Rhine estuary reported in earlier work (Middelburg and Herman,  
464 2007), suggesting intense sediment reworking in connection with harbor expansion over the last 15  
465 years have had little impact on sediment OM sources. Furthermore, the range in observed  $\delta^{13}\text{C}_{\text{org}}$   
466 values is lower than that reported for temperate marine OM (–18 and –22‰; (Thornton and



467 McManus, 1994)), reflecting a significant non-marine OM source even under nearly marine conditions  
468 at the river mouth. Quantification of the different sources using end-member modelling similarly  
469 indicates that the dominant OM source shifts with depositional environment: terrestrial OM in the most  
470 river-dominated locations (up to 65%, salinity < 5), freshwater OM in the river-sea transitional area (~  
471 45%, 5 < salinity < 25), and marine OM in the river-mouth area (up to 65%, salinity > 25).

472

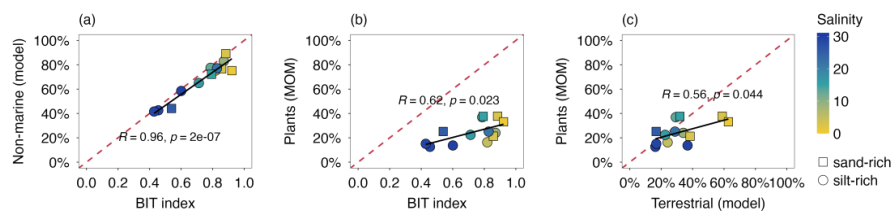
473 Regarding the range of and trend in C/N values, it is important to note that the value is subject to OM-  
474 specific alterations during sediment diagenesis: for higher plant litter, the C/N ratio decreases during  
475 decomposition, while for aquatic detritus the C/N ratio increases during degradation (Hedges and  
476 Oades, 1997; Wakeham and Canuel, 2006). These opposing diagenetic trajectories can result in a  
477 convergence of C/N ratios of terrestrial and aquatic detritus (Middelburg and Herman, 2007). This  
478 may explain bulk sediments at many of the investigated sites in the PoR research area have C/N  
479 ratios near the upper limit of the typical range for freshwater algae (~8) or POC (~10), or around the  
480 lower limit of the typical range for C<sub>3</sub> plants (~12, Fig. 2b). Compared to the C/N ratio, the BIT index is  
481 thought to be less sensitive to diagenetic effects (Hopmans et al., 2004). This proxy indicates a  
482 predominant riverine and/or terrestrial source of the sedimentary OM (Schouten et al., 2013). The BIT  
483 values from this study are in line with the values previously determined by Herfort et al. (2006) in  
484 sediment at Maassluis (0.74–0.82; close to NWWG-09, Fig 1), while they are much higher than those  
485 determined in coastal sediments of the southern North Sea (0.02–0.25; (Herfort et al., 2006)),  
486 highlighting the sharp transition in OM composition between estuarine and coastal systems and the  
487 importance of non-marine OM throughout the harbor system.

488

489 The source proxies presented above ( $\delta^{13}\text{C}_{\text{org}}$ , C/N, BIT) indicate a strong terrestrial and riverine OM  
490 signature across the salinity gradient in the PoR study area, with a considerable marine contribution  
491 at the river mouth. The pyrolysis products from MOM can offer additional insights into sediment OM  
492 sources and composition. Guaiacols and syringols are pyrolytic markers of terrestrial OM, as they are  
493 characteristic structural moieties of lignin, a typical biopolymer of higher plants. Their relative  
494 abundance together (7–28%) falls within the reported lignin fractions (3–57%) for various coastal  
495 aquatic environments (Brandini et al., 2022; Burdige, 2007; Kaal et al., 2020). Although having  
496 multiple potential sources, the markers of polysaccharides in our samples showed strong positive  
497 correlations with both guaiacols ( $R = 0.77$ , Pearson) and syringols ( $R = 0.83$ , Pearson), suggesting  
498 they were mainly derived from terrestrial higher plants. The decreasing trends of these markers  
499 (relative abundance 10–40%) with increasing salinity, well aligned with  $\delta^{13}\text{C}_{\text{org}}$  and BIT index, further  
500 support the decreasing importance of terrestrial OM input towards the river mouth. In contrast, N-  
501 compounds showed strong negative correlations with both guaiacols ( $R = -0.84$ , Pearson) and  
502 syringols ( $R = -0.81$ , Pearson), suggesting a non-terrestrial OM origin such as protein from algal  
503 detritus and chitin from various crustaceans (Nierop et al., 2017). *n*-Alkenes/alkanes, negatively  
504 correlated with (terrestrial) polysaccharide-derived products ( $R = -0.78$ , Pearson; Fig. S3), was  
505 probably from non-terrestrial sources like algaenan (de Leeuw et al., 2006). The other detected  
506 pyrolysis products constituted a major fraction (> 50%) but most correlated with all mentioned source



507 proxies moderately or poorly ( $-0.5 < R < 0.5$ , Pearson; Fig. S3), thus are less effective as source  
508 indicators as they likely originate from multiple, non-negligible sources.  
509  
510 All proxies and analytical techniques have their strengths and weaknesses in determining OM  
511 sources. Here, we obtain further insight into MOM characteristics and the performance of various  
512 techniques by exploring the relationships between different independent OM proxies and the end-  
513 member modelling results. There is a striking agreement between the BIT index and the modelled  
514 non-marine OM contribution ( $R = 0.96$ , Pearson; Fig. 8a). The BIT index is a ratio that corresponds to  
515 the relative importance of marine OM vs. soil and riverine OM. Its strong correlation with the modelled  
516 non-marine OM (encompassing soil OM, riverine OM, and terrestrial vegetation input) suggests that  
517 vegetation input was not a major component of the modelled non-marine OM contribution. Plant-  
518 derived OM, however, was suggested to be a major MOM constituent, with an abundance of lignin-  
519 derived products of up to 40% (Fig. 8b). Possibly, the lignin-derived products were mainly from eroded  
520 soils carrying plenty of OM debris from the plants previously growing on them, or the amount of  
521 vegetation input scaled proportionately with the amount of soil input.  
522  
523 The terrestrial OM fraction modelled from C/N and  $\delta^{13}\text{C}_{\text{org}}$  showed a positive correlation with plant-  
524 derived MOM pyrolysis products (Fig. 8c). Most data points seem to lie around the 1:1 curve except  
525 two sand-rich outliers. However, interpreting their relationship in Fig. 8c is challenging because of the  
526 complexity in assigning MOM pyrolysis products to terrestrial-derived OM in estuarine environment.  
527 Phenols and N-compounds, partially derived from terrestrial OM, are not included in the presented  
528 MOM-determined contribution here. On the other hand, pyrolysis of algal material also produces  
529 polysaccharide-derived products (Stevenson and Abbott, 2019), which can lead to overestimation of  
530 MOM-determined terrestrial contribution. Nevertheless, our study suggests using bulk proxies (C/N,  
531  $\delta^{13}\text{C}_{\text{org}}$ ) in combination with biomarker proxies (BIT index, MOM pyrolysis products) can provide a  
532 more complete picture of OM composition in highly dynamic systems like estuaries.  
533



534  
535 Fig. 8. Scatter plots of proxies for OM source: (a) BIT index vs. non-marine OM contribution (i.e.  
536 terrestrial and riverine input from the three end-member modelling), (b) modelled terrestrial OM  
537 contribution vs. plant-derived MOM pyrolysis products (i.e. sum of guaiacols, syringols,  
538 polysaccharide-derived products), (c) BIT index vs. plant-derived MOM pyrolysis products (i.e. sum of  
539 guaiacols, syringols, polysaccharide-derived products). The red dashed lines are 1:1 curves and the  
540 black lines are the linear regression fitting curves.  
541





#### 542 **4.2 Organic matter degradation: rates and pathways**

543 In the 8-h whole-core incubation experiment, oxygen consumption was mostly due to OM  
544 mineralization; calculation of upward diffusive fluxes of reduced elements that can react with oxygen  
545 (e.g.  $\text{Fe}^{2+}$ ,  $\text{Mn}^{2+}$ ,  $\text{H}_2\text{S}$ ) indicated that this represented a negligible oxygen sink at the sediment-water  
546 interface ( $< 1\%$  of total oxygen uptake; see SI). The measured benthic  $\text{O}_2$  consumption rates were  
547 very similar for sediments from two strongly contrasting environments in the marine and riverine part  
548 of the research area (Fig. 5a). The PoR sediments exhibited similar  $\text{O}_2$  consumption rates ( $33 \pm 6$   
549  $\text{mmol m}^{-2} \text{d}^{-1}$ ) as coastal North Sea sediments ( $22.1 \pm 0.6 \text{ mmol m}^{-2} \text{d}^{-1}$ ; (Neumann et al., 2021)) and  
550 human-influenced estuarine sediment ( $27\text{--}82 \text{ mmol m}^{-2} \text{d}^{-1}$ ; (Kraal et al., 2013)). Generally, sediment  
551 oxygen consumption decreases with increasing water depth from  $45 \pm 22 \text{ mmol m}^{-2} \text{d}^{-1}$  on the inner  
552 shelf to  $0.8 \pm 0.8 \text{ mmol m}^{-2} \text{d}^{-1}$  on the abyssal seafloor due to the increasing fraction of recalcitrant OM  
553 at the deeper realm (Jørgensen et al., 2022). However, when considering OM content in the surface  
554 sediment, the  $\text{O}_2$  consumption rate for sediment 115 (depth  $\sim 25$  m, TOC 2.2 wt.%) is about twice that  
555 of sediment 21A (depth  $\sim 13$  m, TOC 5.0 wt.%). This suggests that OM source and composition as  
556 function of the depositional environment plays a key role in determining carbon oxidation rates and  
557 thereby the functioning of estuarine systems as important  $\text{CO}_2$  sources in the global carbon cycle (Li  
558 et al., 2023).

559  
560 Like  $\text{O}_2$  consumption rates, DIC effluxes from the sediment were similar for the two contrasting sites  
561 (Fig. 5b). However, sediment 115 exhibited a larger TOC-normalized DIC flux (Fig. 5d), likely due to  
562 the greater supply and burial of fresh OM caused by a faster burial rate ( $10\text{--}15 \text{ cm yr}^{-1}$ ) in comparison  
563 to sediment 21A ( $< 10 \text{ cm yr}^{-1}$ ; (Cox et al., 2021). Besides, sediment 21A at the riverine side was  
564 suggested to be richer in the eroded (ancient) soil OM (Fig. 8), often more recalcitrant than freshly  
565 produced OM. The respiratory quotient (RQ), determined as the ratio between DIC outflux and  $\text{O}_2$   
566 influx, was notably higher in our estuarine sediments (3.75–5) than the typical range observed in  
567 marine sediments (0.69–1.31; (Jørgensen et al., 2022), probably because carbonate dissolution  
568 enhances the DIC flux. Correction using DIN flux (Fig. S4) and Redfield ratio (C:N = 106:16) revealed  
569 that only about 40% of DIC was generated from OM degradation (see SI), among which 50–71% was  
570 produced aerobically. The RQ remained relatively high (1.4–2) after DIN correction, highlighting the  
571 importance of anaerobic degradation in shallow coastal systems, compared to the open ocean where  
572 RQs are often less than 1 (Jørgensen et al., 2022).

573  
574 Regarding the role of estuaries in carbon cycling, a crucial transition in anaerobic OM degradation  
575 pathways is the onset of methanogenesis, which occurs when other TEAs have become depleted.  
576 Due to a lower salinity and thus sulfate concentration, sediment from a river location (21A; salinity 5.1)  
577 exhibited an eight-time larger  $\text{CH}_4$  efflux (Fig. 5c) compared to the marine location (115; salinity 28.7)  
578 despite of less degradable OM with a stronger terrestrial signature (Fig. 2) as evidenced by the  
579 above-described lower OM mineralization rates relative to TOC content. Similar spatial variability of  
580 benthic  $\text{CH}_4$  fluxes as function of salinity was documented in other estuaries but with rather different  
581 values (Gelesh et al., 2016; Li et al., 2021; Middelburg et al., 2002). The benthic fluxes measured



582 here do not directly translate into atmospheric CO<sub>2</sub> and CH<sub>4</sub> emissions as various processes (e.g.  
583 carbonate system equilibria, CH<sub>4</sub> oxidation) act on the speciation and concentration of these  
584 greenhouse gases released from the sediment. Nevertheless, estuaries are considered as hotspots  
585 for both CO<sub>2</sub> and CH<sub>4</sub> emissions into atmosphere (Li et al., 2023; Middelburg et al., 2002). Therefore,  
586 elucidating how in addition to OM content the source and composition as well environmental  
587 conditions during OM degradation control the magnitude and speciation of carbon release from  
588 estuarine sediment is important to better constrain the role of estuaries in global carbon cycling.

589

#### 590 **4.3 The impact of perturbation on organic matter degradation**

591 Sediment dredging and its further management, such as relocation on land, often alter OM  
592 degradation conditions substantially by reintroducing O<sub>2</sub>. In principle, aerobic degradation is more  
593 effective than anaerobic degradation as aerobic oxidation has a relatively high energy yield, especially  
594 compared to sulfate reduction (Hansen and Blackburn, 1991). This is reflected in our whole-core  
595 incubation results (Fig. 6) where aerobic mineralization (usually only a few millimeters thick;  
596 (Revsbech et al., 1980)) accounted for 50–71% of the total OM-derived DIC production (~15 cm). By  
597 manually perturbing sediments and exposing them to atmospheric oxygen in subaerial incubations,  
598 we found that the initial (day 2) TOC-normalized carbon emission rate ( $283 \pm 42 \mu\text{mol C g C}^{-1} \text{d}^{-1}$  for  
599 115,  $134 \pm 29 \mu\text{mol C g C}^{-1} \text{d}^{-1}$  for 21A; Fig. 6b) increased to 3.8–8.4 times of that in undisturbed whole-  
600 core incubation ( $74 \pm 10 \mu\text{mol C g C}^{-1} \text{d}^{-1}$  for 115,  $16 \pm 1 \mu\text{mol C g C}^{-1} \text{d}^{-1}$  for 21A; Fig. 5e). These findings  
601 agree with a slurry incubation experiment under contrasting redox conditions using Dutch coastal  
602 sediments conducted by (Dauwe et al., 2001), which showed that the mineralization rate under  
603 aerobic conditions was faster than anaerobic condition by up to one order of magnitude. Furthermore,  
604 the increase in carbon emission rate was more pronounced in the riverine sediment (21A) with a  
605 ~740% increase after perturbation, compared to the marine sediment (115) with a ~280% increase.  
606 We attribute this to the stronger terrestrial, recalcitrant signature of OM in the riverine part of the  
607 investigated harbor area. (Hulthe et al., 1998) suggested that the impact of redox conditions and  
608 specifically oxygen availability is greatest for relatively recalcitrant OM; fresh, labile OM is degraded  
609 relatively rapidly under aerobic and anaerobic conditions. Therefore, the difference in the observed  
610 rate increase following sediment perturbation may be attributed to the more active enzymatic catalysis  
611 involved in the degradation of terrestrial OM, such as lignin, cellulose, and tannins (Hedges and  
612 Oades, 1997), compared to freshly produced marine OM was more predominant. These OM source-  
613 dependent differences in OM degradation rates were expressed across the six investigated sites: the  
614 TOC-normalized carbon emission rates were over 100% higher in marine sediments (115, 86,  
615 NWWG-02) than riverine sediments (21A, B16, K1v2) at almost all timesteps (Fig. 6b). This observed  
616 difference is supported by our OM end-member analysis: sediments near the river mouth (115, 86,  
617 NWWG-02) were composed of more than 50% marine OM and less than 20% terrestrial OM, whereas  
618 sediments from the river side (21A, B16, K1v2) were dominated (>70%) by non-marine OM (Fig. 2c,  
619 Table S2). The faster degradation rate of marine OM, such as algae, which was reported to be up to  
620 10 times as quicker as terrestrial OM (Guillemette et al., 2013), likely explains the higher TOC-  
621 normalized carbon emission rates in marine sediments.



622

623 In addition to the degradation rate, the extent of OM degradation is also affected by the OM source  
624 and composition. By the end of the subaerial incubation experiment, marine sediments (115, 86,  
625 NWWG-02) exhibited 2–4 times larger fractions of degraded TOC than riverine sediments (21A, B16,  
626 K1v2; Fig. 7). Despite a lower TOC content, marine sediments contained a higher percentage of  
627 fresher and more labile OM, thus resulting in a larger biodegradation fraction after 37 days of  
628 subaerial incubation. Interestingly, sand-rich sediment NWWG-02 exhibited a notably larger  
629 biodegradable OM fraction (up to 7%; Fig. 7), highlighting sediment texture may play an important role  
630 besides OM sources. Silt-rich sediment can contain 20 times more mineral-associated OM than  
631 sand-rich wetland soils (Mirabito and Chambers, 2023). This mineral-associated OM, physically  
632 protected by inorganic matrices from mineralization, was suggested to play a key role in lasting  
633 carbon sequestration globally (Georgiou et al., 2022).

634

635 Despite variations in the fractions of degraded TOC, more than 90% of the organic carbon remained  
636 in the sediments by the end of the 37-day aerobic incubation experiments (Fig. 7). This aligns with  
637 other studies where a majority fraction (> 80%) of organic carbon remained preserved in sediments or  
638 soils after prolonged incubation periods ranging from weeks to years (Gebert et al., 2019; Haynes,  
639 2005; Plante et al., 2011). The predominant fraction of sediment OM being less degradable on such  
640 timescales fits well with the relatively large amounts (~50%) of pyrolysis products derived from  
641 (terrestrial) polysaccharide, *n*-alkenes/alkanes from algaenan, guaiacols and syringols from lignin.  
642 However, (Zander et al., 2022) indicated that the slow degradation of the majority of OM could also be  
643 attributed to its association with sedimentary minerals. Importantly, the remaining OM, while resistant  
644 to degradation over weeks to years, is still potentially degradable on longer timescales and relevant  
645 for the carbon footprint of perturbing estuarine sediment over decades. While our and other results  
646 indicate that reintroduction of O<sub>2</sub> leads to a short-lived increase in estuarine OM degradation rates,  
647 the degradation can still be stimulated under certain conditions. For instance, the addition of fresh,  
648 readily degradable OM, known as priming, was reported to increase the degradability of old,  
649 recalcitrant OM by 59% (Huo et al., 2017). This highlights the organic carbon turnover rate is rather  
650 complex and can vary markedly under different sediment management practices.

651

#### 652 **4.4 Implications and future perspectives**

653 Estuaries are sites of high OM production and processing, and understanding biogeochemical  
654 processes within these regions is key to quantify organic carbon budgets along the river-estuary-  
655 coastal ocean continuum (Canuel and Hardison, 2016). The use of multiple proxies (e.g. C/N,  $\delta^{13}\text{C}_{\text{org}}$ ,  
656 biomarkers) can improve our ability to understand, quantify, and predict the fate of organic carbon  
657 delivered from continents to the oceans. Our study demonstrated that OM degradation exhibited a  
658 source-specific pattern where both degradation rate and biodegradable pool varied over few times  
659 depending on the origin of the OM. Degradation of OM is responsible for the recycling of essential  
660 nutrients, for the oxygen balance of the aquatic system and its sediments and for most early  
661 diagenetic processes (Middelburg et al., 1993). Recognizing and differentiating OM reactivity of



662 varying sources can help to refine the biogeochemical processes and minimize the uncertainty in  
663 estimating OM mineralization and preservation efficiency in both field and theoretical frameworks.  
664  
665 Anthropogenic perturbation like dredging within the coastal zone have greatly intensified in recent  
666 decades. Thus, it is crucial to recognize and quantify the impact of these sediment rework on carbon  
667 mineralization. The sediment disturbance could have a considerable impact on the local carbon cycle  
668 by accelerating the release of both CO<sub>2</sub> and CH<sub>4</sub> into the atmosphere (van de Velde et al., 2018).  
669 Generally, the dredged material is relocated either underwater or on land. Exposure of sediment to  
670 oxygenated environment can notably accelerate OM mineralization. When dredged sediment is  
671 applied on land, the loss of the overlying water reduces the retention capacity of DIC, thereby  
672 increasing CO<sub>2</sub> outgassing into atmosphere. Methane, a strong greenhouse gas, is often  
673 oversaturated in the OM-rich coastal sediments where CH<sub>4</sub> bubbles are formed. Depending on the  
674 dredging depth and sediment quality, dredging can lead to a short-term CH<sub>4</sub> emission peak by  
675 increasing diffusion and ebullition (Maeck et al., 2013; Nijman et al., 2022). Estuarine systems are  
676 characterized by a strong salinity gradient with a large variability of the depth of the sedimentary  
677 methanic zone. Anaerobic oxidation of methane consumes approximately 71% of the CH<sub>4</sub> in marine  
678 sediments (Gao et al., 2022), while dredging will inevitably disrupt anaerobic methane oxidation.  
679 Further research should quantify the effect of dredging on CH<sub>4</sub> emission under realistic, large scale  
680 dredging practices. Whether dredging activities can change the ecological service of estuarine  
681 sediment from a carbon sink into a carbon source depends on the initial sediment carbon dynamics  
682 as well as the intensity of human disturbance. Indubitably, estuaries will remain vulnerable to human  
683 pressure and climate change. These alternations will in return influence the important drivers of the  
684 estuarine, further affecting the balance between OM degradation and preservation (Heckbert et al.,  
685 2012).

686

## 687 **Conclusions**

- 688 • Applying multiple proxies from independent analyses gained a more comprehensive picture of the  
689 OM sources and composition in highly dynamic environments such as estuaries. Here, the  
690 combination of CN proxies, BIT index, and flash pyrolysis of MOM suggested the increasing  
691 marine input and decreasing riverine and terrestrial input along a salinity gradient in the PoR area  
692 located in a major European estuarine system. Throughout the salinity transition from freshwater  
693 to nearly marine condition, considerable marine, riverine, and terrestrial (mostly eroded soil)  
694 signals were detected at all locations. Consistency between the BIT index and CN based end-  
695 member modelling suggested the robustness of the CN proxies and lipid biomarker in  
696 distinguishing marine and non-marine OM contributions, whereas pyrolysis products of MOM are  
697 suitable for assessing relative abundances of certain compounds (e.g. lignin) in a coastal  
698 environment.
- 699 • The PoR sediments, like many other coastal sediments, exhibited relatively high OM content and  
700 reactivity, probably because of the high primary production and rapid sedimentation rate in these



701 shallow aquatic systems. However, TOC-normalized carbon release/production rates showed OM  
702 degradation was significantly faster in marine sediments than in riverine sediments under both  
703 intact conditions and disturbed oxygenated conditions, suggesting marine OM was more  
704 susceptible to degradation. This is likely because marine sediment contained larger amount of  
705 recently formed more labile OM. Higher sedimentation rates at the marine side contribute to a  
706 better preservation of relatively fresher OM. In contrast, riverine sediments contain larger amounts  
707 of eroded, ancient soil OM, possibly decades to centuries old, with only the more recalcitrant  
708 fraction surviving by the time they reach the investigated locations. It highlights OM source and  
709 composition, age, and sedimentation rate might be the key to the systematic explanation of OM  
710 susceptibility in our study area.

- 711 • Nevertheless, OM degradability is not an inherent characteristic of OM itself, but also dependent  
712 on the environmental context. Sediment perturbation with O<sub>2</sub> reintroduction showed to  
713 substantially increase OM degradation by 2.8–7.4 times compared to intact conditions. With the  
714 increasing intensity in coastal engineering, it is important to recognize the need to apply carbon-  
715 sensitive management for sediments. Despite the degraded TOC being only 1–7% after 37-day  
716 oxic incubation, the remaining organic carbon can still be turned over under certain conditions.  
717 Therefore, quantifying organic carbon stability requires consideration of the relevant timescale as  
718 well as that of the fast-changing environmental conditions.

719  
720  
721  
722



723 **Author contribution**

724 GW conceptualized the study, developed the methodology, conducted the investigation and formal  
725 analysis, created visualizations, and wrote the original draft of the manuscript. KN and BY contributed  
726 to the investigation and formal analysis, and reviewed and edited the manuscript. SS and GJR  
727 reviewed and edited the manuscript. PK supervised the project, contributed to the conceptualization  
728 and methodology, acquired funding, and reviewed and edited the manuscript. All authors reviewed  
729 and agreed on the final version of the manuscript.

730

731 **Data availability**

732 The datasets used in this study are available from the corresponding author upon reasonable request.

733

734 **Declaration of competing interest**

735 The authors declare no competing interests.

736

737 **Acknowledgements**

738 This study is part of the project 'Transforming harbor sediment from waste into resource' funded by  
739 the Exact and Natural Sciences domain of the Dutch Research Council, NWO (grant number  
740 TWM.BL.019.005). We extend our gratitude to the Port of Rotterdam Authority, particularly Marco  
741 Wensveen and Ronald Rutgers, and Heijdra Milieu Service B.V. for their assistance with sediment  
742 collection. We thank Julia Gebert from Delft University of Technology for her stimulating discussion.  
743 We appreciate the scientific and technical staff from NIOZ Royal Netherlands Institute for Sea  
744 Research for their analytical support.

745

746 **Appendix A. Supplementary data**

747 The online version contains supplementary material available at XXX.

748

749

750



## 751 References

- 752 Aller, R. C.: Bioturbation and remineralization of sedimentary organic matter: effects of redox  
753 oscillation, *Chemical Geology*, 114, 331–345, [https://doi.org/10.1016/0009-2541\(94\)90062-0](https://doi.org/10.1016/0009-2541(94)90062-0), 1994.
- 754 Aller, R. C., Blair, N. E., Xia, Q., and Rude, P. D.: Remineralization rates, recycling, and storage of  
755 carbon in Amazon shelf sediments, *Continental Shelf Research*, 16, 753–786,  
756 [https://doi.org/10.1016/0278-4343\(95\)00046-1](https://doi.org/10.1016/0278-4343(95)00046-1), 1996.
- 757 Amar, M., Benzerzour, M., Kleib, J., and Abriak, N. E.: From dredged sediment to supplementary  
758 cementitious material: characterization, treatment, and reuse, *International Journal of Sediment*  
759 *Research*, 36, 92–109, <https://doi.org/10.1016/j.ijsrc.2020.06.002>, 2021.
- 760 Arndt, S., Jørgensen, B. B., LaRowe, D. E., Middelburg, J. J., Pancost, R. D., and Regnier, P.:  
761 Quantifying the degradation of organic matter in marine sediments: A review and synthesis, *Earth-*  
762 *Science Reviews*, 123, 53–86, <https://doi.org/10.1016/j.earscirev.2013.02.008>, 2013.
- 763 Barbier, E. B., Hacker, S. D., Kennedy, C., Koch, E. W., Stier, A. C., and Silliman, B. R.: The value of  
764 estuarine and coastal ecosystem services, *Ecological Monographs*, 81, 169–193,  
765 <https://doi.org/10.1890/10-1510.1>, 2011.
- 766 Bauer, J. E., Cai, W. J., Raymond, P. A., Bianchi, T. S., Hopkinson, C. S., and Regnier, P. A. G.: The  
767 changing carbon cycle of the coastal ocean, *Nature*, 504, 61–70, <https://doi.org/10.1038/nature12857>,  
768 2013.
- 769 Bianchi, T. S. and Bauer, J. E.: Particulate Organic Carbon Cycling and Transformation, Elsevier Inc.,  
770 69–117 pp., <https://doi.org/10.1016/B978-0-12-374711-2.00503-9>, 2012.
- 771 Bianchi, T. S., Cui, X., Blair, N. E., Burdige, D. J., Eglinton, T. I., and Galy, V.: Centers of organic  
772 carbon burial and oxidation at the land-ocean interface, *Organic Geochemistry*, 115, 138–155,  
773 <https://doi.org/10.1016/j.orggeochem.2017.09.008>, 2018.
- 774 Brandini, N., da Costa Machado, E., Sanders, C. J., Cotovicz, L. C., Bernardes, M. C., and Knoppers,  
775 B. A.: Organic matter processing through an estuarine system: Evidence from stable isotopes ( $\delta^{13}\text{C}$   
776 and  $\delta^{15}\text{N}$ ) and molecular (lignin phenols) signatures, *Estuarine, Coastal and Shelf Science*, 265,  
777 <https://doi.org/10.1016/j.ecss.2021.107707>, 2022.
- 778 Brils, J., de Boer, P., Mulder, J., and de Boer, E.: Reuse of dredged material as a way to tackle  
779 societal challenges, *Journal of Soils and Sediments*, 14, 1638–1641, <https://doi.org/10.1007/s11368-014-0918-0>, 2014.
- 781 Burd, A. B., Frey, S., Cabre, A., Ito, T., Levine, N. M., Lønborg, C., Long, M., Mauritz, M., Thomas, R.  
782 Q., Stephens, B. M., Vanwallegem, T., and Zeng, N.: Terrestrial and marine perspectives on  
783 modeling organic matter degradation pathways, *Global Change Biology*, 22, 121–136,  
784 <https://doi.org/10.1111/gcb.12987>, 2016.
- 785 Burdige, D. J.: Preservation of organic matter in marine sediments: Controls, mechanisms, and an  
786 imbalance in sediment organic carbon budgets?, *Chemical Reviews*, 107, 467–485,  
787 <https://doi.org/10.1021/cr050347q>, 2007.
- 788 Burdige, D. J.: Estuarine and Coastal Sediments - Coupled Biogeochemical Cycling, Elsevier Inc.,  
789 279–316 pp., <https://doi.org/10.1016/B978-0-12-374711-2.00511-8>, 2012.
- 790 Buurman, P., Nierop, K. G. J., Pontevedra-Pombal, X., and Martínez Cortizas, A.: Chapter 10  
791 Molecular chemistry by pyrolysis-GC/MS of selected samples of the Penido Vello peat deposit,  
792 Galicia, NW Spain, *Developments in Earth Surface Processes*, 9, 217–240,  
793 [https://doi.org/10.1016/S0928-2025\(06\)09010-9](https://doi.org/10.1016/S0928-2025(06)09010-9), 2006.
- 794 Canuel, E. A. and Hardison, A. K.: Sources, Ages, and Alteration of Organic Matter in Estuaries,  
795 *Annual Review of Marine Science*, 8, 409–434, <https://doi.org/10.1146/annurev-marine-122414-034058>, 2016.
- 797 Cao, C., Cai, F., Qi, H., Zhao, S., and Wu, C.: Differences in the sulfate–methane transitional zone in  
798 coastal pockmarks in various sedimentary environments, *Water (Switzerland)*, 13, 1–18,  
799 <https://doi.org/10.3390/w13010068>, 2021.
- 800 Carneiro, L. M., do Rosário Zucchi, M., de Jesus, T. B., da Silva Júnior, J. B., and Hadlich, G. M.:  
801  $\delta^{13}\text{C}$ ,  $\delta^{15}\text{N}$  and TOC/TN as indicators of the origin of organic matter in sediment samples from the  
802 estuary of a tropical river, *Marine Pollution Bulletin*, 172,  
803 <https://doi.org/10.1016/j.marpolbul.2021.112857>, 2021.
- 804 Chow, W. L., Chong, S., Lim, J. W., Chan, Y. J., Chong, M. F., Tiong, T. J., Chin, J. K., Pan, G. T.,  
805 Puyuelo, B., Ponsá, S., Gea, T., Sánchez, A., Szulc, W., Rutkowska, B., Gawroński, S., and  
806 Wszelaczyńska, E.: Determining C/N ratios for typical organic wastes using biodegradable fractions,  
807 *Processes*, 85, 653–659, <https://doi.org/10.3390/pr9091501>, 2020.
- 808 Cloern, J. E., Canuel, E. A., and Harris, D.: Stable carbon and nitrogen isotope composition of aquatic  
809 and terrestrial plants of the San Francisco Bay estuarine system, *Limnology and Oceanography*, 47,  
810 713–729, <https://doi.org/10.4319/lo.2002.47.3.0713>, 2002.



- 811 Cox, J. R., Dunn, F. E., Nienhuis, J. H., van der Perk, M., and Kleinhans, M. G.: Climate change and  
812 human influences on sediment fluxes and the sediment budget of an urban delta: The example of the  
813 lower rhine–meuse delta distributary network, *Anthropocene Coasts*, 4, 251–280,  
814 <https://doi.org/10.1139/anc-2021-0003>, 2021.
- 815 Dauwe, B., Middelburg, J. J., and Herman, P. M. J.: Effect of oxygen on the degradability of organic  
816 matter in subtidal and intertidal sediments of the North Sea area, 215, 13–22, 2001.
- 817 Dürr, H. H., Laruelle, G. G., van Kempen, C. M., Slomp, C. P., Meybeck, M., and Middelkoop, H.:  
818 Worldwide Typology of Nearshore Coastal Systems: Defining the Estuarine Filter of River Inputs to  
819 the Oceans, *Estuaries and Coasts*, 34, 441–458, <https://doi.org/10.1007/s12237-011-9381-y>, 2011.
- 820 Fabbri, D., Sangiorgi, F., and Vassura, I.: Pyrolysis-GC-MS to trace terrigenous organic matter in  
821 marine sediments: A comparison between pyrolytic and lipid markers in the Adriatic Sea, *Analytica  
822 Chimica Acta*, 530, 253–261, <https://doi.org/10.1016/j.aca.2004.09.020>, 2005.
- 823 Fairbairn, L., Rezanezhad, F., Gharasoo, M., Parsons, C. T., Macrae, M. L., Slowinski, S., and Van  
824 Cappellen, P.: Relationship between soil CO<sub>2</sub> fluxes and soil moisture: Anaerobic sources explain  
825 fluxes at high water content, *Geoderma*, 434, 116493,  
826 <https://doi.org/10.1016/j.geoderma.2023.116493>, 2023.
- 827 Finlay, J. C. and Kendall, C.: Stable Isotope Tracing of Temporal and Spatial Variability in Organic  
828 Matter Sources to Freshwater Ecosystems, in: *Stable Isotopes in Ecology and Environmental  
829 Science*, edited by: Michener, R. and Lajtha, Wiley, 283–333,  
830 <https://doi.org/10.1002/9780470691854.ch10>, 2007.
- 831 Freitas, F. S., Pika, P. A., Kasten, S., Jorgensen, B. B., Rassmann, J., Rabouille, C., Thomas, S.,  
832 Sass, H., Pancost, R. D., and Arndt, S.: New insights into large-scale trends of apparent organic  
833 matter reactivity in marine sediments and patterns of benthic carbon transformation, *Biogeosciences*,  
834 18, 4651–4679, <https://doi.org/10.5194/bg-18-4651-2021>, 2021.
- 835 Gao, Y., Wang, Y., Lee, H. S., and Jin, P.: Significance of anaerobic oxidation of methane (AOM) in  
836 mitigating methane emission from major natural and anthropogenic sources: a review of AOM rates in  
837 recent publications, *Environmental Science: Advances*, 1, 401–425,  
838 <https://doi.org/10.1039/d2va00091a>, 2022.
- 839 Gebert, J., Knoblauch, C., and Gröngroft, A.: Gas production from dredged sediment, *Waste  
840 Management*, 85, 82–89, <https://doi.org/10.1016/j.wasman.2018.12.009>, 2019.
- 841 Gelesh, L., Marshall, K., Boicourt, W., and Lapham, L.: Methane concentrations increase in bottom  
842 waters during summertime anoxia in the highly eutrophic estuary, Chesapeake Bay, U.S.A.,  
843 *Limnology and Oceanography*, 61, S253–S266, <https://doi.org/10.1002/lno.10272>, 2016.
- 844 Georgiou, K., Jackson, R. B., Vindušková, O., Abramoff, R. Z., Ahlström, A., Feng, W., Harden, J. W.,  
845 Pellegrini, A. F. A., Polley, H. W., Soong, J. L., Riley, W. J., and Torn, M. S.: Global stocks and  
846 capacity of mineral-associated soil organic carbon, *Nature Communications*, 13, 1–12,  
847 <https://doi.org/10.1038/s41467-022-31540-9>, 2022.
- 848 Guillemette, F., McCallister, S. L., and Del Giorgio, P. A.: Differentiating the degradation dynamics of  
849 algal and terrestrial carbon within complex natural dissolved organic carbon in temperate lakes,  
850 *Journal of Geophysical Research: Biogeosciences*, 118, 963–973, <https://doi.org/10.1002/jgrg.20077>,  
851 2013.
- 852 Hansen, L. S. and Blackburn, T. H.: Aerobic and anaerobic mineralization of organic material in  
853 marine sediment microcosms, *Marine Ecology Progress Series*, 75, 283–291,  
854 <https://doi.org/10.3354/meps075283>, 1991.
- 855 Haynes, R. J.: Labile Organic Matter Fractions as Central Components of the Quality of Agricultural  
856 Soils: An Overview, *Advances in Agronomy*, 85, 221–268, [https://doi.org/10.1016/S0065-  
857 2113\(04\)85005-3](https://doi.org/10.1016/S0065-2113(04)85005-3), 2005.
- 858 Heckbert, S., Costanza, R., Poloczanska, E. S., and Richardson, A. J.: Climate Regulation as a  
859 Service from Estuarine and Coastal Ecosystems, Elsevier Inc., 199–216 pp.,  
860 <https://doi.org/10.1016/B978-0-12-374711-2.01211-0>, 2012.
- 861 Hedges, J. I. and Oades, J. M.: Comparative organic geochemistries of soils and marine sediments,  
862 *Organic Geochemistry*, 27, 319–361, [https://doi.org/10.1016/S0146-6380\(97\)00056-9](https://doi.org/10.1016/S0146-6380(97)00056-9), 1997.
- 863 Herfort, L., Schouten, S., Boon, J. P., Woltering, M., Baas, M., Weijers, J. W. H., and Sinninghe  
864 Damsté, J. S.: Characterization of transport and deposition of terrestrial organic matter in the southern  
865 North Sea using the BIT index, *Limnology and Oceanography*, 51, 2196–2205,  
866 <https://doi.org/10.4319/lno.2006.51.5.2196>, 2006.
- 867 Holligan, P. M. and Reiners, W. A.: Predicting the Responses of the Coastal Zone to Global Change,  
868 *Advances in Ecological Research*, 22, 211–255, [https://doi.org/10.1016/S0065-2504\(08\)60137-3](https://doi.org/10.1016/S0065-2504(08)60137-3),  
869 1992.





- 870 Hopmans, E. C., Weijers, J. W. H., Schefuß, E., Herfort, L., Sinninghe Damsté, J. S., and Schouten,  
871 S.: A novel proxy for terrestrial organic matter in sediments based on branched and isoprenoid  
872 tetraether lipids, *Earth and Planetary Science Letters*, 224, 107–116,  
873 <https://doi.org/10.1016/j.epsl.2004.05.012>, 2004.
- 874 Hopmans, E. C., Schouten, S., and Sinninghe Damsté, J. S.: The effect of improved chromatography  
875 on GDGT-based palaeoproxies, *Organic Geochemistry*, 93, 1–6,  
876 <https://doi.org/10.1016/j.orggeochem.2015.12.006>, 2016.
- 877 Hulthe, G., Hulth, S., and Hall, P. O. J.: Effect of oxygen on degradation rate of refractory and labile  
878 organic matter in continental margin sediments, *Geochimica et Cosmochimica Acta*, 62, 1319–1328,  
879 [https://doi.org/10.1016/S0016-7037\(98\)00044-1](https://doi.org/10.1016/S0016-7037(98)00044-1), 1998.
- 880 Huo, C., Luo, Y., and Cheng, W.: Rhizosphere priming effect: A meta-analysis, *Soil Biology and*  
881 *Biochemistry*, 111, 78–84, <https://doi.org/10.1016/j.soilbio.2017.04.003>, 2017.
- 882 IJsseldijk, L. L., Camphuysen, K. C. J., Nauw, J. J., and Aarts, G.: Going with the flow: Tidal influence  
883 on the occurrence of the harbour porpoise (*Phocoena phocoena*) in the Marsdiep area, The  
884 Netherlands, *Journal of Sea Research*, 103, 129–137, <https://doi.org/10.1016/j.seares.2015.07.010>,  
885 2015.
- 886 Jørgensen, B. B., Wenzhöfer, F., Egger, M., and Glud, R. N.: Sediment oxygen consumption: Role in  
887 the global marine carbon cycle, *Earth-Science Reviews*, 228,  
888 <https://doi.org/10.1016/j.earscirev.2022.103987>, 2022.
- 889 Kaal, J.: Analytical pyrolysis in marine environments revisited, *Analytical Pyrolysis Letters*, 1–16,  
890 2019.
- 891 Kaal, J., Martínez Cortizas, A., Mateo, M. Á., and Serrano, O.: Deciphering organic matter sources  
892 and ecological shifts in blue carbon ecosystems based on molecular fingerprinting, *Science of the*  
893 *Total Environment*, 742, 140554, <https://doi.org/10.1016/j.scitotenv.2020.140554>, 2020.
- 894 Keil, R., Montluçon, D., Prahl, F., and Hedges, J.: Sorptive preservation of labile organic matter in  
895 marine sediments, *Nature*, 370, 549–552, <https://doi.org/https://doi-org.utrechtuniversity.idm.oclc.org/10.1038/370549a0>, 1994.
- 897 Kirichek, A. and Rutgers, R.: Monitoring of settling and consolidation of mud after water injection  
898 dredging in the Calandkanaal, *Terra et Aqua*, 160, 16–26, 2020.
- 899 Kraal, P., Burton, E. D., Rose, A. L., Cheetham, M. D., Bush, R. T., and Sullivan, L. A.: Decoupling  
900 between water column oxygenation and benthic phosphate dynamics in a shallow eutrophic estuary,  
901 *Environmental Science and Technology*, 47, 3114–3121, <https://doi.org/10.1021/es304868t>, 2013.
- 902 Kuwae, T., Kanda, J., Kubo, A., Nakajima, F., Ogawa, H., Sohma, A., and Suzumura, M.: Blue carbon  
903 in human-dominated estuarine and shallow coastal systems, *Ambio*, 45, 290–301,  
904 <https://doi.org/10.1007/s13280-015-0725-x>, 2016.
- 905 Lamb, A. L., Wilson, G. P., and Leng, M. J.: A review of coastal palaeoclimate and relative sea-level  
906 reconstructions using  $\delta^{13}\text{C}$  and C/N ratios in organic material, *Earth-Science Reviews*, 75, 29–57,  
907 <https://doi.org/10.1016/j.earscirev.2005.10.003>, 2006.
- 908 LaRowe, D. E. and Van Cappellen, P.: Degradation of natural organic matter: A thermodynamic  
909 analysis, *Geochimica et Cosmochimica Acta*, 75, 2030–2042,  
910 <https://doi.org/10.1016/j.gca.2011.01.020>, 2011.
- 911 LaRowe, D. E., Arndt, S., Bradley, J. A., Estes, E. R., Hoarfrost, A., Lang, S. Q., Lloyd, K. G.,  
912 Mahmoudi, N., Orsi, W. D., Shah Walter, S. R., Steen, A. D., and Zhao, R.: The fate of organic carbon  
913 in marine sediments - New insights from recent data and analysis, *Earth-Science Reviews*, 204,  
914 103146, <https://doi.org/10.1016/j.earscirev.2020.103146>, 2020.
- 915 Laruelle, G. G., Dürr, H. H., Slomp, C. P., and Borges, A. V.: Evaluation of sinks and sources of CO<sub>2</sub>  
916 in the global coastal ocean using a spatially-explicit typology of estuaries and continental shelves,  
917 *Geophysical Research Letters*, 37, 1–6, <https://doi.org/10.1029/2010GL043691>, 2010.
- 918 de Leeuw, J. W., Versteegh, G. J. M., and van Bergen, P. F.: Biomacromolecules of algae and plants  
919 and their fossil analogues, *Plant Ecology*, 182, 209–233, <https://doi.org/10.1007/s11258-005-9027-x>,  
920 2006.
- 921 Li, M., Guo, Y., Cai, W. J., Testa, J. M., Shen, C., Li, R., and Su, J.: Projected increase in carbon  
922 dioxide drawdown and acidification in large estuaries under climate change, *Communications Earth*  
923 *and Environment*, 4, 1–10, <https://doi.org/10.1038/s43247-023-00733-5>, 2023.
- 924 Li, Y., Zhan, L., Chen, L., Zhang, J., Wu, M., and Liu, J.: Spatial and temporal patterns of methane  
925 and its influencing factors in the Jiulong River estuary, southeastern China, *Marine Chemistry*, 228,  
926 103909, <https://doi.org/10.1016/j.marchem.2020.103909>, 2021.
- 927 Macreadie, P. I., Anton, A., Raven, J. A., Beaumont, N., Connolly, R. M., Friess, D. A., Kelleway, J. J.,  
928 Kennedy, H., Kuwae, T., Lavery, P. S., Lovelock, C. E., Smale, D. A., Apostolaki, E. T., Atwood, T. B.,  
929 Baldock, J., Bianchi, T. S., Chmura, G. L., Eyre, B. D., Fourqurean, J. W., Hall-Spencer, J. M.,



- 930 Huxham, M., Hendriks, I. E., Krause-Jensen, D., Laffoley, D., Luisetti, T., Marbà, N., Masque, P.,  
931 McGlathery, K. J., Megonigal, J. P., Murdiyarso, D., Russell, B. D., Santos, R., Serrano, O., Silliman,  
932 B. R., Watanabe, K., and Duarte, C. M.: The future of Blue Carbon science, *Nature Communications*,  
933 10, 1–13, <https://doi.org/10.1038/s41467-019-11693-w>, 2019.
- 934 Maeck, A., Delsontro, T., McGinnis, D. F., Fischer, H., Flury, S., Schmidt, M., Fietzek, P., and Lorke, A.:  
935 Sediment trapping by dams creates methane emission hot spots, United States of America,  
936 *Environmental Science and Technology*, 8130–8137, 2013.
- 937 Magen, C., Lapham, L. L., Pohlman, J. W., Marshall, K., Bosman, S., Casso, M., and Chanton, J. P.: A  
938 simple headspace equilibration method for measuring dissolved methane, *Limnology and*  
939 *Oceanography: Methods*, 12, 637–650, <https://doi.org/10.4319/lom.2014.12.637>, 2014.
- 940 McLeod, E., Chmura, G. L., Bouillon, S., Salm, R., Björk, M., Duarte, C. M., Lovelock, C. E.,  
941 Schlesinger, W. H., and Silliman, B. R.: A blueprint for blue carbon: Toward an improved  
942 understanding of the role of vegetated coastal habitats in sequestering CO<sub>2</sub>, *Frontiers in Ecology and*  
943 *the Environment*, 9, 552–560, <https://doi.org/10.1890/110004>, 2011.
- 944 Middelburg, J. J. and Herman, P. M. J.: Organic matter processing in tidal estuaries, *Marine*  
945 *Chemistry*, 106, 127–147, <https://doi.org/10.1016/j.marchem.2006.02.007>, 2007.
- 946 Middelburg, J. J. and Nieuwenhuize, J.: Carbon and nitrogen stable isotopes in suspended matter and  
947 sediments from the Schelde Estuary, *Marine Chemistry*, 60, 217–225, [https://doi.org/10.1016/S0304-4203\(97\)00104-7](https://doi.org/10.1016/S0304-4203(97)00104-7), 1998.
- 949 Middelburg, J. J., Vlуг, T., Jaco, F., and van der Nat, W. A.: Organic matter mineralization in marine  
950 systems, *Global and Planetary Change*, 8, 47–58, [https://doi.org/10.1016/0921-8181\(93\)90062-S](https://doi.org/10.1016/0921-8181(93)90062-S),  
951 1993.
- 952 Middelburg, J. J., Nieuwenhuize, J., Iversen, N., Høgh, N., De Wilde, H., Helder, W., Seifert, R., and  
953 Christof, O.: Methane distribution in European tidal estuaries, *Biogeochemistry*, 59, 95–119,  
954 <https://doi.org/10.1023/A:1015515130419>, 2002.
- 955 Mirabito, A. J. and Chambers, L. G.: Quantifying mineral-associated organic matter in wetlands as an  
956 indicator of the degree of soil carbon protection, *Geoderma*, 430, 116327,  
957 <https://doi.org/10.1016/j.geoderma.2023.116327>, 2023.
- 958 Neumann, A., van Beusekom, J. E. E., Eisele, A., Emeis, K. C., Friedrich, J., Kröncke, I., Logemann,  
959 E. L., Meyer, J., Naderipour, C., Schückel, U., Wrede, A., and Zettler, M. L.: Macrofauna as a major  
960 driver of benthic-pelagic exchange in the southern North Sea, *Limnology and Oceanography*, 66,  
961 2203–2217, <https://doi.org/10.1002/lno.11748>, 2021.
- 962 Nierop, K. G. J., Reichart, G. J., Veld, H., and Sinninghe Damsté, J. S.: The influence of oxygen  
963 exposure time on the composition of macromolecular organic matter as revealed by surface  
964 sediments on the Murray Ridge (Arabian Sea), *Geochim Cosmochim Acta*, 206, 40–56,  
965 <https://doi.org/10.1016/j.gca.2017.02.032>, 2017.
- 966 Nijman, T. P. A., Lemmens, M., Lurling, M., Kosten, S., Welte, C., and Veraart, A. J.: Phosphorus  
967 control and dredging decrease methane emissions from shallow lakes, *Science of the Total*  
968 *Environment*, 847, 157584, <https://doi.org/10.1016/j.scitotenv.2022.157584>, 2022.
- 969 Plante, A. F., Fernández, J. M., Haddix, M. L., Steinweg, J. M., and Conant, R. T.: Biological, chemical  
970 and thermal indices of soil organic matter stability in four grassland soils, *Soil Biology and*  
971 *Biochemistry*, 43, 1051–1058, <https://doi.org/10.1016/j.soilbio.2011.01.024>, 2011.
- 972 Puyuelo, B., Ponsá, S., Gea, T., and Sánchez, A.: Determining C/N ratios for typical organic wastes  
973 using biodegradable fractions, *Chemosphere*, 85, 653–659,  
974 <https://doi.org/10.1016/j.chemosphere.2011.07.014>, 2011.
- 975 Revsbech, N. P., Sorensen, J., Blackburn, T. H., and Lomholt, J. P.: Distribution of oxygen in marine  
976 sediments measured with microelectrodes, *Limnology and Oceanography*, 25, 403–411,  
977 <https://doi.org/10.4319/lo.1980.25.3.0403>, 1980.
- 978 Schouten, S., Hopmans, E. C., and Sinninghe Damsté, J. S.: The organic geochemistry of glycerol  
979 dialkyl glycerol tetraether lipids: A review, *Organic Geochemistry*, 54, 19–61,  
980 <https://doi.org/10.1016/j.orggeochem.2012.09.006>, 2013.
- 981 Schulz, H. and Zabel, M.: *Marine Geochemistry*, Springer Berlin Heidelberg New York, 132 pp., 2006.
- 982 Shao, L., Wu, D., Zhang, D., and Feng, T.: Using Isotopes to Identify the Sources of Organic Carbon  
983 and Nitrogen in Surface Sediment in Shallow Lakes Alongside Poyang Lake, *Wetlands*, 39, 25–33,  
984 <https://doi.org/10.1007/s13157-017-0988-z>, 2019.
- 985 Smith, R. W., Bianchi, T. S., and Savage, C.: Comparison of lignin phenols and branched/isoprenoid  
986 tetraethers (BIT index) as indices of terrestrial organic matter in Doubtful Sound, Fiordland, New  
987 Zealand, *Organic Geochemistry*, 41, 281–290, <https://doi.org/10.1016/j.orggeochem.2009.10.009>,  
988 2010.



- 989 Steele, J. H., Thorpe, S. A., and Turekian, K. K.: Marine Chemistry & Geochemistry, edited by: Steele,  
990 J. H., Thorpe, S. A., and Turekian, K. K., 2010.
- 991 Stevenson, M. A. and Abbott, G. D.: Exploring the composition of macromolecular organic matter in  
992 Arctic Ocean sediments under a changing sea ice gradient, *Journal of Analytical and Applied*  
993 *Pyrolysis*, 140, 102–111, <https://doi.org/10.1016/j.jaap.2019.02.006>, 2019.
- 994 Stock, B. C., Jackson, A. L., Ward, E. J., Parnell, A. C., Phillips, D. L., and Semmens, B. X.: Analyzing  
995 mixing systems using a new generation of Bayesian tracer mixing models, *PeerJ*, 2018, 1–27,  
996 <https://doi.org/10.7717/peerj.5096>, 2018.
- 997 Strong, D. J., Flecker, R., Valdes, P. J., Wilkinson, I. P., Rees, J. G., Zong, Y. Q., Lloyd, J. M., Garrett,  
998 E., and Pancost, R. D.: Organic matter distribution in the modern sediments of the Pearl River  
999 Estuary, *Organic Geochemistry*, 49, 68–82, <https://doi.org/10.1016/j.orggeochem.2012.04.011>, 2012.
- 1000 Stronkhorst, J. and Van Hattum, B.: Contaminants of concern in Dutch marine harbor sediments,  
1001 *Archives of Environmental Contamination and Toxicology*, 45, 306–316,  
1002 <https://doi.org/10.1007/s00244-003-0191-5>, 2003.
- 1003 Szulc, W., Rutkowska, B., Gawroński, S., and Wszelaczyńska, E.: Possibilities of using organic waste  
1004 after biological and physical processing—an overview, *Processes*, 9,  
1005 <https://doi.org/10.3390/pr9091501>, 2021.
- 1006 Thornton, S. F. and McManus, J.: Application of organic carbon and nitrogen stable isotope and C/N  
1007 ratios as source indicators of organic matter provenance in estuarine systems: Evidence from the tay  
1008 estuary, Scotland, *Estuarine, Coastal and Shelf Science*, 38, 219–233,  
1009 <https://doi.org/10.1006/ecss.1994.1015>, 1994.
- 1010 Tumuluru, J. S., Hess, J. R., Boardman, R. D., Wright, C. T., and Westover, T. L.: Formulation,  
1011 pretreatment, and densification options to improve biomass specifications for Co-firing high  
1012 percentages with coal, *Industrial Biotechnology*, 8, 113–132, <https://doi.org/10.1089/ind.2012.0004>,  
1013 2012.
- 1014 van de Velde, S., van Lancker, V., Hidalgo-Martinez, S., Berelson, W. M., and Meysman, F. J. R.:  
1015 Anthropogenic disturbance keeps the coastal seafloor biogeochemistry in a transient state, *Scientific*  
1016 *Reports*, 8, 1–10, <https://doi.org/10.1038/s41598-018-23925-y>, 2018.
- 1017 Wakeham, S. G. and Canuel, E. A.: Degradation and preservation of organic matter in marine  
1018 sediments, *Handbook of Environmental Chemistry, Volume 2: Reactions and Processes*, 2 N, 295–  
1019 321, [https://doi.org/10.1007/698\\_2\\_009](https://doi.org/10.1007/698_2_009), 2006.
- 1020 Wiesner, M. G., Haake, B., and Wirth, H.: Organic facies of surface sediments in the North Sea,  
1021 *Organic Geochemistry*, 15, 419–432, [https://doi.org/10.1016/0146-6380\(90\)90169-Z](https://doi.org/10.1016/0146-6380(90)90169-Z), 1990.
- 1022 Yamamoto, S., Alcauskas, J. B., and Crozier, T. E.: Solubility of Methane in Distilled Water and  
1023 Seawater, *Journal of Chemical and Engineering Data*, 21, 78–80,  
1024 <https://doi.org/10.1021/je60068a029>, 1976.
- 1025 Zander, F., Heimovaara, T., and Gebert, J.: Spatial variability of organic matter degradability in tidal  
1026 Elbe sediments, *Journal of Soils and Sediments*, 20, 2573–2587, <https://doi.org/10.1007/s11368-020-02569-4>, 2020.
- 1027  
1028 Zander, F., Groengroeft, A., Eschenbach, A., Heimovaara, T. J., and Gebert, J.: Organic matter pools  
1029 in sediments of the tidal Elbe river, *Limnologia*, 96, 125997,  
1030 <https://doi.org/10.1016/j.limno.2022.125997>, 2022.
- 1031